29 Appendix Q – Fish Barriers

Table 85. A list of roads identified as having barriers to fish migration. Acronyms used in this table are identified in Appendix M – ODF Roads Protocol.

Route ID	Distance	Material	Structural Type	Fish Presence	Restriction of fish passage
JUNO	14760	STELC	RPIPE	F	AB
BDAM	35555	STELC	PARCH	F	FB
BDAM6.45	1535	STELC	PARCH	F	FB
1S-9-18.2	2600	UWOOD	BRIDG	L	AB
BDAM	9715	STELC	RPIPE	L	AB
BDAM	28550	STELC	RPIPE	L	AB
BDAM	30625	STELC	RPIPE	L	AB
BVR	2580	STELC	RPIPE	L	AB
CLIN	3225	STELC	RPIPE	L	AB
KNS CK	3165	STELC	PARCH	L	AB
KNS CK	3860	STELC	PARCH	L	AB
LAMT1.37	695	STELC	RPIPE	L	AB
MUESL	5665	STELC	RPIPE	L	AB
N FK WIL	10415	STELC	PARCH	L	AB
POLLO	2950	SBEAM	RPIPE	L	AB
SAD2	3950	STELC	RPIPE	L	AB
SCCK0.53	790	STELC	RPIPE	L	AB
SFWI	24335	STELC	RPIPE	L	AB
1-7-11	4350	STELC	PARCH	L	FB
1-7-9.2	125	STELC	RPIPE	L	FB
BDAM	21025	STELC	RPIPE	L	FB
BDAM	24400	STELC	PARCH	L	FB
BDAM	26270	STELC	PARCH	L	FB
DRCK	24345	STELC	RPIPE	L	FB
IDCK1.56A	2425	STELC	RPIPE	L	FB
KILCH LO	7675	STELC	RPIPE	L	FB
SCCK	8335	STELC	PARCH	L	FB
SMITH	2960	STELC	RPIPE	L	FB
1-6-18	3335	STELC	RPIPE	U	AB
1-8-1.4	2895	STELC	RPIPE	U	AB
1-8-1.4	3875	STELC	RPIPE	U	AB
1-8-12.1	1255	STELC	RPIPE	U	AB
1S-8-11.0	4855	PLAST	RPIPE	U	AB
1S-8-11.4	2760	STELC	RPIPE	U	AB
1S-8-2.1	20	STELC	RPIPE	U	AB
1S-8-2.2	905	STELC	RPIPE	U	AB
1S-8-2.2	1235	STELC	RPIPE	U	AB
1S-9-9.1	195	ALUMN	RPIPE	U	AB
ARCHERS	22345	STELC	RPIPE	U	AB
ARCHERS	39355	STELC	RPIPE	U	AB
BD5R	2990	STELC	RPIPE	U	AB
BDAM	6120	STELC	RPIPE	U	AB

Route ID	Distance	Material	Structural Type	Fish Presence	Restriction of fish passage
BDAM	13790	STELC	RPIPE	U	AB
BDAM	32105	STELC	PARCH	U	AB
BDAM1.08	1130	STELC	RPIPE	U	AB
BDAM6.45B1	1320	STELC	RPIPE	U	AB
BDAM6.45F	365	STELC	RPIPE	U	AB
BEN SMITH	1675	STELC	RPIPE	U	AB
BEN SMITH	8670	STELC	RPIPE	U	AB
BEN SMITH	9285	STELC	RPIPE	U	AB
BVR	4245	STELC	RPIPE	U	AB
BVR	4915	STELC	RPIPE	U	AB
CDR CK	10585	CONCR	RPIPE	U	AB
CDR CK	11335	STELC	RPIPE	U	AB
CDR CK	12930	STELC	RPIPE	U	AB
CDR CK	16420	STELC	RPIPE	U	AB
CDR CK	17465	STELC	RPIPE	U	AB
CDR CK	19380	STELC	RPIPE	U	AB
CDR CK	23820	STELC	RPIPE	U	AB
CHIC	6030	STELC	RPIPE	U	AB
CLIN	20025	STELC	RPIPE	U	AB
CLIN	22760	STELC	RPIPE	U	AB
CLIN	38400	STELC	RPIPE	U	AB
CLIN	40075	STELC	RPIPE	U	AB
CLIN	43485	STELC	RPIPE	U	AB
CLIN	45860	STELC	PARCH	U	AB
CST RNG LP2	855	STELC	RPIPE	U	AB
CST RNG N	1585	STELC	RPIPE	U	AB
CST RNG N	1905	STELC	RPIPE	U	AB
CST RNG N	4835	STELC	RPIPE	U	AB
CST RNG N	5845	STELC	RPIPE	U	AB
CST RNG N	6550	STELC	RPIPE	U	AB
D FNCE	13245	STELC	RPIPE	U	AB
DRCK	22330	STELC	RPIPE	U	AB
DRCK	26265	STELC	RPIPE	U	AB
DRCK	38610	STELC	RPIPE	U	AB
EAID	5745	STELC	RPIPE	U	AB
FALL CK	260	PLAST	RPIPE	U	AB
FALL CK	2225	STELC	RPIPE	U	AB
IDCK	1345	STELC	RPIPE	U	AB
IDCK0.43	4305	STELC	RPIPE	U	AB
IDCK1.56	7835	STELC	RPIPE	U	AB
IDCK1.56A	2125	STELC	RPIPE	U	AB
JORDAN CK	9015	STELC	RPIPE	U	AB
JORDAN CK	13700	STELC	RPIPE	U	AB
JORDAN CK	33990	STELC	RPIPE	U	AB
JORDAN CK	53955	STELC	RPIPE	U	AB
JUNO	13015	STELC	RPIPE	U	AB
KILCH LO	5305	STELC	RPIPE	U	AB

Route ID	Distance	Material	Structural Type	Fish Presence	Restriction of fish passage
KNS CK	1180	STELC	RPIPE	U	AB
KNS CK	5050	STELC	RPIPE	U	AB
LAMT	6490	STELC	RPIPE	U	AB
MILLS_BRDG	3992	STELC	RPIPE	U	AB
MUESL	9495	STELC	RPIPE	U	AB
MUESL	9715	STELC	RPIPE	U	AB
MUESL	10865	STELC	RPIPE	U	AB
N FK WIL	1910	STELC	RPIPE	U	AB
N FK WIL	7305	STELC	RPIPE	U	AB
N FK WIL	7670	STELC	RPIPE	U	AB
N FK WIL	10320	STELC	RPIPE	U	AB
N FK WIL	12265	STELC	RPIPE	U	AB
NF WF	1955	ALUMN	RPIPE	U	AB
NF WF	6425	STELC	RPIPE	U	AB
NF WF	16795	STELC	RPIPE	U	AB
OLD CDR	5060	STELC	RPIPE	U	AB
POLLO	725	STELC	RPIPE	U	AB
POLLO	2730	STELC	RPIPE	U	AB
POWERLINE1	1385	ALUMN	RPIPE	U	AB
POWERLINE10	1810	STELC	RPIPE	U	AB
POWERLINE11	960	STELC	RPIPE	U	AB
RUTH2.20	1265	STELC	RPIPE	U	AB
SAD1-1.14	9880	STELC	RPIPE	U	AB
SCCK0.53	3835	STELC	RPIPE	U	AB
SFWI	11675	STELC	RPIPE	U	AB
SFWI	16160	STELC	RPIPE	U	AB
SFWI1.42	5745	STELC	RPIPE	U	AB
SFWI1.42	7070	STELC	RPIPE	U	AB
SFWI1.42A	805	ALUMN	RPIPE	U	AB
SFWI3.52C	1635	STELC	RPIPE	U	AB
SFWI3.52C	2410	STELC	RPIPE	U	AB
SFWI7.38	325	STELC	RPIPE	U	AB
SMITH	3330	STELC	RPIPE	U	AB
SUGARLF	6515	STELC	RPIPE	U	AB
SUGARLF	7170	STELC	RPIPE	U	AB
SUGARLF	7280	STELC	RPIPE	U	AB
SUGARLF	9495	STELC	RPIPE	U	AB
UFAL	20095	STELC	RPIPE	U	AB
UFAL	22775	STELC	RPIPE	U	AB
UFAL	33815	STELC	RPIPE	U	AB
UFAL4.13	935	STELC	RPIPE	U	AB
W FK WIL	4005	STELC	RPIPE	U	AB
WOLFCREEKRD	12065	STELC	RPIPE	U	AB
YANKEE	4575	STELC	RPIPE	U	AB
1-8-12.1	1365	STELC	RPIPE	U	FB
1-8-25.2	1920	STELC	RPIPE	U	FB
1S-8-2.2	105	STELC	RPIPE	U	FB

Route ID	Distance	Material	Structural Type	Fish Presence	Restriction of fish passage
	440	ALUMN	RPIPE	U	FB
	4325	STELC	RPIPE	U	FB
NG N	9910	STELC	RPIPE	U	FB
NO	14280	STELC	RPIPE	U	FB
	8455	STELC	RPIPE	U	FB
	4880	STELC	RPIPE	U	FB
	5505	STELC	RPIPE	U	FB
	6385	STELC	RPIPE	U	FB

Table 86. Results of the GIS exercise to determine quantity of potential habitat blocked by barriers. This method is only an estimate of miles because of the inconsistencies of the location of where streams lie in the ODFW layer and how stream-crossing data were collected. First, no metadata is available at this time to accurately characterize the stream layer. Secondly, when field crews surveyed crossings they did not refer to a stream map. They recorded the distance of the stream from the road beginning and recorded the crossings attributes (see Road Sediment Appendix for Data collection protocol). Once the stream crossings were "attached" to a routed road layer they may or may not line up with the existing stream layer. The routed road layer is calibrated to identifiable features on the ground; however, streams were not one of those features because of the unknown spatial accuracy of the stream layer. The first stage of the spatial query involves selecting all stream crossings that are within 200 feet of fish bearing streams in the ODFW stream layer. Then a subjective manual procedure was carried out that selected from the selected stream crossings those that "made sense" in terms of being related to fish bearing streams. Then a determination was made as to the number of those selected from the selected in terms of their relation to ODFW designations of "assumed" and "verified" fish bearing streams. The results are contained in 4 spatial point layers, NFDCA, UFDCA, LFDCA, FSHDCA.

	No Fish	**Unlikely Fish**	**Likely Fish**	**Fish**	**Total**
Number in Data Base	689	146	59	32	926
Selected Within 200 Feet of Fish bearing streams	165	69	56	31	
Actual number associated with fish bearing stream	36	40	51	30	
Number Associated With Assumed	24	24	14	3	
Number Associated With Verified	12	16	38	27	
Point layer name	**NFDCA**	**UFDCA**	**LFDCA**	**FSHDCA**	

Table 87. Stream crossings from which distances were calculated in the field for potentially blocked habitat. These data are dependent on the spatial query outlined above. One reason there are so fewer than Table 1 above is that many barriers were recorded on the same streams but are distributed vertically (upstream to downstream) along different roads.

Road name	Distance	Age class blocked	Distance Upstream Blocked (feet)	ODFW Fish presence verification	Field survey fish presence call
KNS CK	3166 (3860)	Adult Barrier	5457	Assumed	Likely fish bearing
SFWI	24335	Adult Barrier	3426	Assumed	Likely fish bearing
IDCK1.56A	2425	Juvenile barrier	4106	Assumed	Likely fish bearing
SCCK	8335	Juvenile barrier	7241	Assumed	Likely fish bearing
1S-8-2.1	20	Adult Barrier	551	Assumed	Unlikely fish bearing

Road name	Distance	Age class blocked	Distance Upstream Blocked (feet)	ODFW Fish presence verification	Field survey fish presence call
BDAM	30625	Adult Barrier	100	Assumed	Unlikely fish bearing
BDAM 1.08	1130	Adult Barrier	680	Assumed	Unlikely fish bearing
BDAM 1.08	9715	Adult Barrier	685	Assumed	Unlikely fish bearing
CHIC	6030	Adult Barrier	1500	Assumed	Unlikely fish bearing
CHIC	6030	Adult Barrier	1955	Assumed	Unlikely fish bearing
CLIN	45860	Adult Barrier	5400	Assumed	Unlikely fish bearing
CLIN	40075	Adult Barrier	1970	Assumed	Unlikely fish bearing
CLIN	22760	Adult Barrier	1640	Assumed	Unlikely fish bearing
CLIN	3225	Adult Barrier	363	Assumed	Unlikely fish bearing
D FNCE	13245	Adult Barrier	985	Assumed	Unlikely fish bearing
DRCK	22330	Adult Barrier	3865	Assumed	Unlikely fish bearing
IDCK1.56	7835	Adult Barrier	100	Assumed	Unlikely fish bearing
KNS CK	5050	Adult Barrier	5870	Assumed	Unlikely fish bearing
LAMT 1.37	695	Adult Barrier	2560	Assumed	Unlikely fish bearing
N FK WIL	12265	Adult Barrier	3500	Assumed	Unlikely fish bearing
NF WF	1955	Adult Barrier	1490	Assumed	Unlikely fish bearing
POWERLINE 1	1385	Adult Barrier	211	Assumed	Unlikely fish bearing
SFWI	11675	Adult Barrier	550	Assumed	Unlikely fish bearing
SFWI1.42	805	Adult Barrier	3384	Assumed	Unlikely fish bearing
SFWI3.52C	1635	Adult Barrier	980	Assumed	Unlikely fish bearing
DRCK	24345	Juvenile barrier	10200	Assumed	Unlikely fish bearing
DRCK	38610	Adult Barrier	3460	Verfied	Unlikely fish bearing
JUNO	14760	Adult Barrier	2,850	Verified	Fish bearing
BVR	2580	Adult Barrier	750	Verified	Likely fish bearing
KNS CK	3165 (3860)	Adult Barrier	2215	Verified	Likely fish bearing
N FK WIL	10415	Adult Barrier	8576	Verified	Likely fish bearing
SCCK0.53	790	Adult Barrier	2940	Verified	Likely fish bearing

Road name	Distance	Age class blocked	Distance Upstream Blocked (feet)	ODFW Fish presence verification	Field survey fish presence call
1-7-11	4350	Juvenile barrier	1470	Verified	Likely fish bearing
1-7-9.2	125	Juvenile barrier	4450	Verified	Likely fish bearing
BDAM	26270	Juvenile barrier	6200	Verified	Likely fish bearing
BDAM	24440	Juvenile barrier	6100	Verified	Likely fish bearing
KILCH LO	7675	Juvenile barrier	2300	Verified	Likely fish bearing
BD5R	2990	Adult Barrier	3230	Verified	Unlikely fish bearing
POLLO (Upstream of Pollo 620)	725	Adult Barrier	720	Verified	Unlikely fish bearing
1-8-25.2	1920	Juvenile barrier	455	Verified	Unlikely fish bearing
BDAM	21790	Juvenile barrier	600	Verified	Unlikely fish bearing
BDAM	21025	Juvenile barrier	8000	Verified	Unlikely fish bearing
BVR	4325	Juvenile barrier	100	Verified	Unlikely fish bearing
SFWI2.65	4880	Juvenile barrier	600	Verified	Unlikely fish bearing
BDAM	35555	Adult Barrier	3475	Assumed	Unlikely fish bearing
BDAM6.45	1535	Juvenile barrier	2400	Assumed	Unlikely fish bearing

This page left intentionally blank.

30 Appendix R – NetMap Analysis of Critical Road Locations

Methods/Background *553*
Roads and Shallow Landslide Potential 553
Roads and Debris Flow Potential 553
Roads and High Quality Habitats 555
Results…. *555*
Roads and Shallow Landslide Potential 555
Roads and Debris Flow Potential 555
Roads and High Quality Habitats 555

The Sediment Source section of this document (Chapter 7) contains a detailed GIS-based analysis of road conditions from the extensive road survey conducted by Duck Creek Associates in 2006 (refer to section 7.4). This appendix contains an additional road analysis conducted using NetMap software.

30.1.1 Methods/Background

Roads and Shallow Landslide Potential

Roads can be a major contributor to habitat problems in watersheds through chronic surface erosion, landsliding, and migration barriers. In managed watersheds, overall road density can be high (2 to 6 km km^{-2}) and it can be difficult to identify all road crossings (of streams) that may be of concern for maintenance, flood watch, reconstruction, or abandonment. For example, in a 100-km^2 watershed under intense management, there can be 200 to 300 kilometers of roads with dozens to hundreds of road crossings of streams, many of which may be steep and prone to landslides and debris flows.

NetMap includes a tool for evaluating roads with respect to the specific properties of the hillslope it crosses, in particular erosion potential. The analysis in the Wilson River watershed uses the grid point parameter of shallow landslide susceptibility. Road segments (cut at 10-m pixel boundaries) are classified according to the landslide density prediction of the hillslopes upon which the road segment is located. Such a prediction does not address the stability of the road itself, including cut or fill slopes.

Roads and Debris Flow Potential

NetMap is also used to evaluate road crossings with respect to debris flow potential. In this analysis, all headwater stream segments that are crossed by a road are delineated and the channel segments (100–m average length) are classified according to debris flow susceptibility. This allows evaluation of whether road-related landslide potential has the ability to trigger a debris flow in

headwater streams or if debris flows (triggered above the road) threaten a road crossing. This is accomplished by viewing, at the same time, both search parameters and identifying overlaps between high road related erosion potential with high debris flow potential in headwater streams (Figure 1).

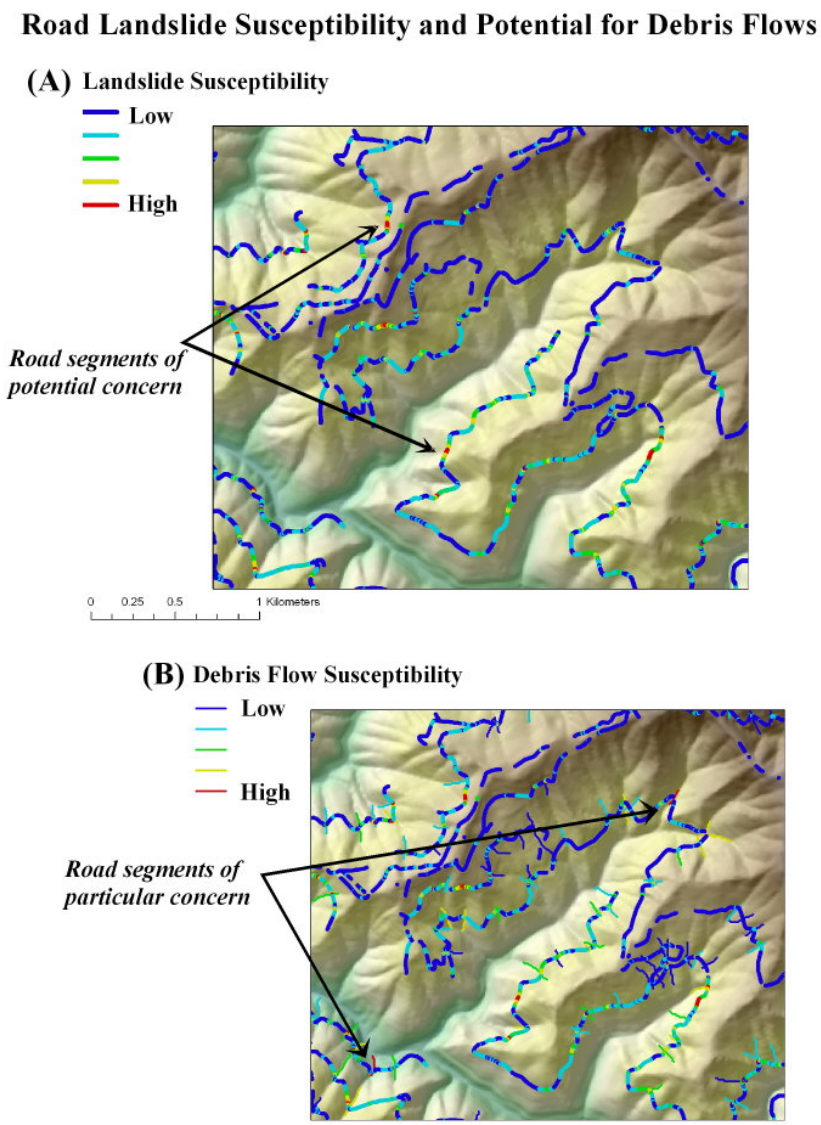

Figure 1. In the Wilson River watershed analysis, NetMap was used to search for road segments that cross hillslopes that have a higher susceptibility to landsliding (A). The road segments (cut at pixel boundaries) are ranked according to the underlying shallow landslide susceptibility rating. Road crossing relationships to debris flow potential in channels (B) can be combined with road-landslide susceptibility (A) to identify particularly sensitive areas.

Roads and High Quality Habitats

Roads that cross high quality and sensitive habitats may also be of concern regarding fish passage and road surface erosion. NetMap is applied to this question by identifying all roads that cross fish-bearing streams in the Wilson River watershed and classifying those channel segments (100-m average length scale) according to Habitat Intrinsic Potential (IP) for coho salmon and steelhead trout.

30.1.2 Results

Roads and Shallow Landslide Potential

Road segments that are located on hillslopes with high landslide potential are fairly common but isolated mainly to upper first- and second-order headwater basins. The distribution of road segments classified according to shallow landslide susceptibility in the Wilson River watershed was divided into three categories based on the analysis of shallow landslide potential values associated with actual landslides.

The average landslide susceptibility value associated with actual landslides was 8.1. The three road-related shallow landslide susceptibility classes are: 0 – 5 (virtually no shallow landsliding was observed on aerial photos), 5 – 8 (corresponds to landsliding values less than the mean), and greater than 8 (corresponds to shallow landsliding values greater than the mean). The relative proportion of road segments in the Wilson River watershed proper that falls into the three landslide susceptibility classes is: 97.6%, 1.1%, and 1.2%. These values pertain to all landslide density values greater than zero, and thus do not include roads on relatively flat ground (valley floors etc.).

Roads and Debris Flow Potential

In this analysis, all stream segments (in headwater basins) that are crossed by a road are identified and classified according to their debris flow susceptibility rating. Identified stream segments (crossed by roads in basins less than 1 km^2, the general limit of debris flow occurrence) range from high to low debris flow susceptibility. Recall that debris flow susceptibility values associated with actual debris flows observed on aerial photography provided a way to evaluate predicted debris flow susceptibility values and to consider preliminary hazard categories. Based on actual debris flow occurrences in the Wilson River watershed and in adjacent basins, susceptibility values ranged from 0.013 to 0.14 with an average of 0.058. The identified stream segments were grouped into three classes of debris flow susceptibility based on that data: values less than the minimum observed (26% of all segments crossed by a road), values between the

mean and the minimum (56% of all segments crossed by a road), and values greater than the mean (18% of all segments crossed by a road).

Roads and High Quality Habitats

In this NetMap analysis, all stream segments that are crossed by a road (along the fish bearing network) are classified according to a specified fish habitat index. Habitat indices used were Habitat Intrinsic Potential (IP) for coho and steelhead (see Section 4.1 and Maps 15 and 16). Road crossings with the highest IP for coho are concentrated along a few areas mostly along the mainstem Wilson River and at the eastern edge of the basin that contains a high concentration of coho habitat.

The same analysis using steelhead IP reveals many more roads that intersect high quality steelhead habitat, with many of the crossings located in the major Wilson River tributaries.

31 Appendix S – Field Validation of Some NetMap Parameters

During this watershed analysis, several NetMap parameters were measured in the field to evaluate their accuracy.

31.1 Methods/Background

The "Field Link" tool in NetMap was used to compare the values of model predicted terrain attributes with field measurements and observations. Using a Toughbook field computer linked to GPS, NetMap's Field Link tool was used to identify channel segments and to cross reference field measured attributes with the corresponding model predicted attributes for the same channel segment. In the field a clinometer was used to measure gradient, a laser rangefinder was used to measure valley width (@ 5X bank full depth), and channel types, wood accumulation types, and habitat intrinsic potential were classified according to non numerical field indictors.

31.2 Results

Field measured parameters are listed in Table 1 (n=24 data points). Comparisons between NetMap predicted parameters and field measurements of those parameters are plotted in Figure 1. There is fairly good agreement between NetMap and field measurements of channel gradient ($r^2 = 0.76$) (Figure 1A). Similarly, NetMap channel widths and field measured widths were comparable ($r^2 = 0.89$) (Figure 1B). The comparison between NetMap valley widths and field-measured channel widths reveals more scatter with only an r^2 of 0.40 (Figure 1C); errors are approximately 50% and NetMap predictions reflect both underestimates and overestimates. The predicted wood accumulation types and field observations show 100% agreement (Table 1). This may be the result of the field validation exercise focusing on relatively small tributary channels (i.e., not mainstem channels).

As indicated in other validation exercises involving the models used in NetMap (Clark and Burnett 2003), the terrain models provide more accurate estimates of watershed attributes in a relativistic sense, rather than highly accurate absolute values. However, at the scale of large watersheds where NetMap is run primarily for evaluating general patterns of attributes such as fish habitat, slope stability, and erosion sources and for large-scale screening purposes, relative accuracy is sufficient. However, where high levels of accuracy in measures of channel gradients, valley widths, and erosion potential etc. are needed, field measurements are recommended.

Table 1. NetMap field validation results are tabulated for channel gradient, channel width, valley width, near stream roughness, and wood accumulation type.

REACH_ID	USER_ID		T_GRAD	F_GRAD	T_CHWIDTH	F_CHWIDTH	T_VW	F_VW	F_VWCW	T_VWCW	T_ROUGHNES	F_ROUGHNES	F_BEDROCK	T_WOOD	F_WO
	22329	1	0.0002	0.001	24.2		100.7		4.16		0.5634			2	
Smith Cree	3546	1	0.0548	0.04	5.1	8	41.2	30	8.12	4	0.1951	75/25	n	2	2
Kansas Cre	4176	2	0.0771	0.07	5	6	22.5	30	4.53		0.3336	0.8/0.7	n	2	2
Kansas Cre	4108	3	0.0347	0.06	6.6	6	26.8	25	4.05		0.3958	60/30	n	2	2
Wilson Riv	4227	4	0.0002		43.4	60	146.8	80	3.38		0.4292	40/40	n	3	3
	7816	5	0.0607	0.08	5.7	10	34.2	16	5.96		0.4064	50/50	n	2	2
Jordan Cre	7815	6	0.0185	na	15.8	12	46.4	16	2.94		0.5432	80/50		2	2
Phipps Cre	7598	7	0.0354	0.04	9.2	10	32.2	35	3.5		0.4673	70/70	n	2	
	7227	8	0.0649	0.08	6.3	5	38.3	17	6.09		0.3331	70/70	n	2	2
South Fork	6654	9	0.0329	0.035	11.2	10	46.5	50	4.14		0.4268	30/20		2	2
W Fk of N	12949	10	0.0318	0.04	12	12	38.5	40	3.22		0.4589	30/70		2	2
Rogers Cre	13505	11	0.039	0.04	11.9	12	32.8		2.75		0.5294	90/20		2	2
W Fk of N	12874	12	0.0277	0.025	17	18	50.2	60	2.95		0.4962	80/50	n	2	2
North Fork	11708	13	0.0177	0.025	16.4	12	55.6	30	3.38		0.6461	90/20	na	2	2
	9966	14	0.0888	0.16	2.1	2	16.1	20	7.49		0.4035	80/80	n	1	1
Cedar Cree	9973	15	0.0341	0.025	9	12	38.3	70	4.25		0.2706	30/15	n	2	2
	9753	16	0.0419	0.05	7.2	8	39	33	5.42		0.247	45/10	na	2	2
Cedar Cree	9702	17	0.0079	.02	13.9	13	55.5	60	3.99		0.3943	60/60	na	2	2
	9532	18	0.0669	0.08	4.2	6	26.8	20	6.39		0.327	80/80	na	2	2
Cedar Cree	9393	19	0.0055	0.015	15.5	22	65	100	4.18		0.3621	20/5	n	2	2
	15807	20	0.0755	0.08	4.2	3	26.8	13	6.35		0.3222	50/80	na	2	2
South Fork	16128	21	0.0374	0.08	12.6	8	43.7	30	3.47		0.2831	80/80	y	2	2
South Fork	15520	22	0.0115	0.015	16.4	18	43.9	41	2.68		0.583	20/80	n	2	2
Devils Lak	16685	23	0.0245	0.015	17.8	18	50.7	40	2.84		0.5316	30/80	na	2	2

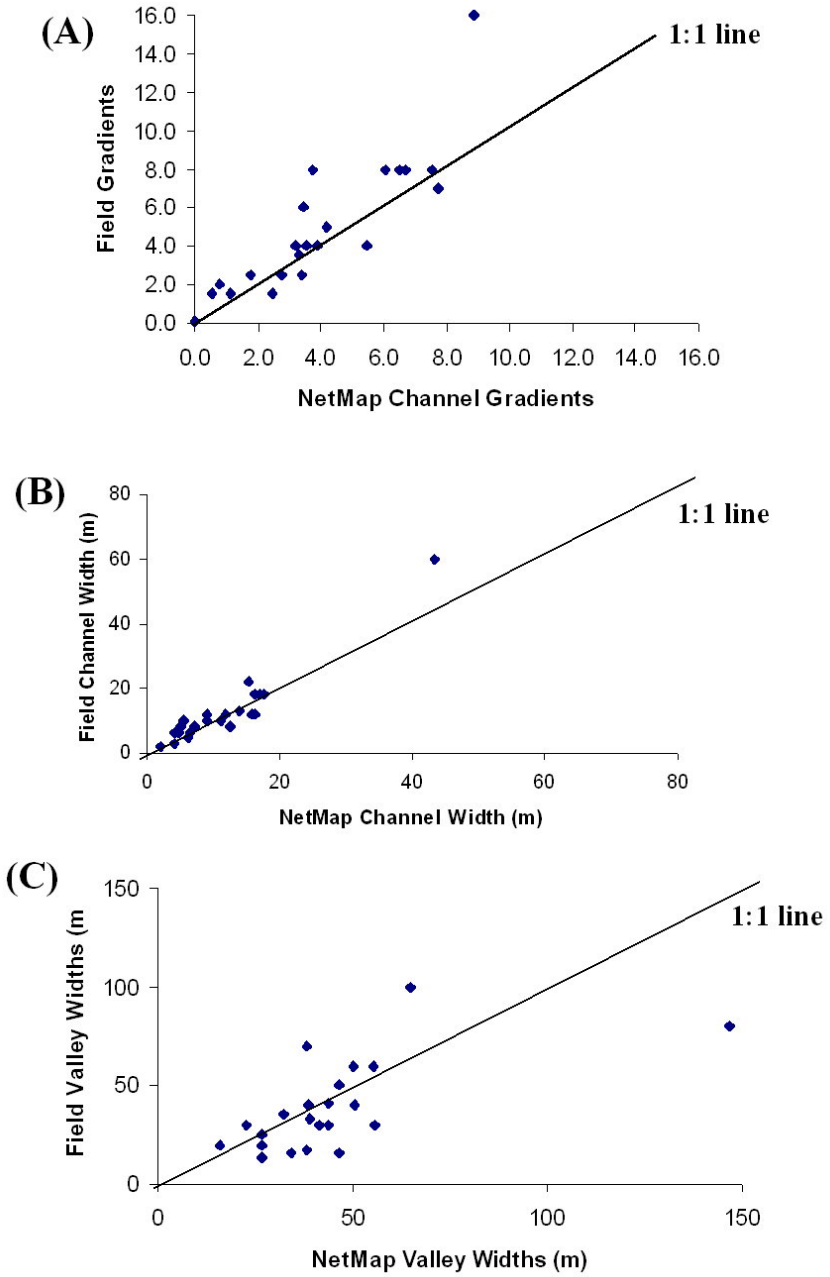

Figure 1. Comparisons between some NetMap watershed attributes and field measured attributes reveal relatively good agreement.

Note that NetMap contains a "field link" tool that can be used to manually override NetMap predictions in the data attribute tables or to create calibration functions to make NetMap parameter values more accurate. In this way, NetMap model predictions can be made more accurate over time.

32 Appendix T – Slope Stability Assessment

32.1 REQUIREMENTS: 561
32.2 STRATEGY: 561
32.3 BACKGROUND: SLOPE STABILITY 562
32.3.1 Relative landslide density to assess topographic controls on slope stability 562
32.3.2 Model evaluation 565
32.3.3 Translation to hazard classes 566
32.3.4 Data and results for the Wilson River Basin 567
32.3.5 Hazard ratings for landslide initiation 570
32.4 DEBRIS-FLOW RUNOUT 570
32.4.1 Topographic factors 570
32.4.2 Model calibration and evaluation 571
32.4.3 Delivery probability 572
32.4.4 Incorporation of delivery probability into hazard ratings 573
32.4.5 Identification of debris-flow-prone Type N channels 574
32.4.6 Debris-Flow-Prone Type F Streams 576
32.5 REFERENCES 578

32.1 Requirements:

- An empirically calibrated, GIS-implemented, and easily interpreted measure of landslide susceptibility and potential for delivery of sediment and wood to streams.
- Interpretation of calculated susceptibility in terms of hazard levels.
- Identification of potential debris-flow-track reaches

32.2 Strategy:

- Use landslide density as a measure of susceptibility to landslide initiation. Quantify effects of topography on landslide density in terms of a weighting function:

  $$\rho = \bar{\rho} w$$

  where ρ is the landslide density to apply locally (e.g., for a DEM cell), $\bar{\rho}$ is mean landslide density (for, e.g., the basin, the region), and w, is a weighting term that quantifies the local influence of topography.

- Empirical calibration: landslide density is determined from mapping on aerial photographs or field surveys overlain on GIS data for topography (derived from DEMs). Analyses are guided by mechanistic models, but this is an empirical model based on extrapolation of observed relationships to similar conditions in areas with no calibration data.
- Resolve influences to the finest detail available, but seek the most widely applicable model. Wide applicability provides simplicity and consistency, but can result in smoothing of local details. In some areas landslide susceptibility will be under predicted, in others it will be over predicted.

- Spatially distributed estimates of the weighting term can be stored as a GIS raster file. Analyses to assess landslide potential then involve simple sums and products of these raster files. The results can be displayed at the resolution of the raster (typically 10 m if 10-m DEMs are used to characterize topography) and may also be aggregated to characterize landslide potential over any specified area.

32.3 Background: slope stability

32.3.1 Relative landslide density to assess topographic controls on slope stability

Landslide locations indicate spatial controls on landslide occurrence. Fewer landslides occur on stable slopes than on unstable slopes, so we gauge susceptibility to landslide occurrence in terms of the relative number of landslides found in different topographic locations.

If we consider landslide density ρ in terms of the number of landslides per unit area, then multiplication of landslide density by area translates to a number of landslides. In a raster GIS context, the number of landslides N expected over any area is simply a sum over cells:

$$N = \bar{\rho} \sum a_c \tag{1}$$

where $\bar{\rho}$ is the mean landslide density (in terms of number per unit area) for all cells and a_c is the area of a cell. By characterizing spatial variations in landslide density, the number of landslides can be calculated as

$$N = a_c \sum \rho_i \tag{2}$$

where cell area a_c, assumed equal for all cells, is removed from the sum, and ρ_i is the landslide density associated with the ith cell.

To characterize spatial variations in landslide density arising from topographic factors, consider a basin of total area A_T with a total number of mapped landslides N_T. These values define a mean landslide density: $\bar{\rho} = N_T/A_T$. The number of landslides n_i mapped over a single gradient class (e.g., 70% to 80%) that occupies an area a_i define a landslide density $\rho_i = n_i/a_i$ specific to that gradient class (see Figure 64, which illustrates these calculations using data from the ODF 1996 Storm Study).

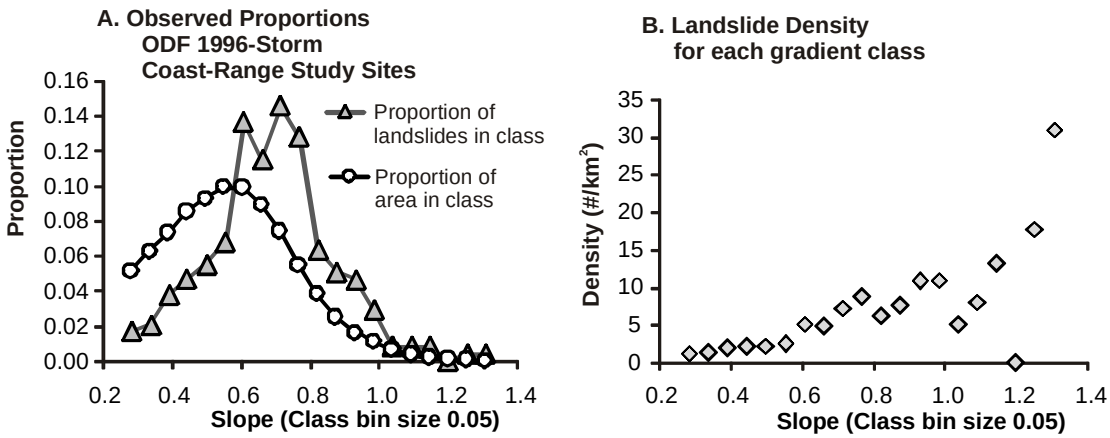

Figure 64. A. The proportion of landslide initiation points and the proportion of study area in each of 20 slope classes for data from the Mapleton, Scottsburg, Elk Creek, Tillamook, and Dalles 1996 Storm study sites (Robison, Mills et al. 1999). B. The landslide density for each of these slope classes.

Now consider n_i and a_i in terms of the proportion they represent of all landslides and of the total study area to define a term w_i (Figure 65a):

$$w_i = \frac{\left(\frac{n_i}{N_T}\right)}{\left(\frac{a_i}{A_T}\right)} = \frac{\rho_i}{\bar{\rho}} \tag{3}$$

Equation 3 shows that w_i gives the magnitude of landslide density observed for the ith class relative to the mean landslide density over all classes. In terms of w_i, ρ_i is given as

$$\rho_i = \frac{n_i}{a_i} = w_i\left(\frac{N_T}{A_T}\right) = w_i\bar{\rho} \tag{4}$$

The term w_i adjusts the mean landslide density depending on whether the density of landslides over that range of gradients was greater than ($w_i > 1$) or less than ($w_i < 1$) the average density. By specifying gradient classes, we can define a value w_i for each class. Each DEM cell occupies a specific gradient class, thereby associating a w_i value to each cell. The terms w_i act to weight the mean landslide density to account for the effects of slope gradient. The number of landslides expected over any specified area (set of cells) can now be calculated as (Figure 65b)

$$N = \bar{\rho} a_c \sum w_i \tag{5}$$

with w_i the weighting value of the ith cell. As N is given by the product of landslide density and area, we can think of $a_c \sum w_i$ as a weighted area.

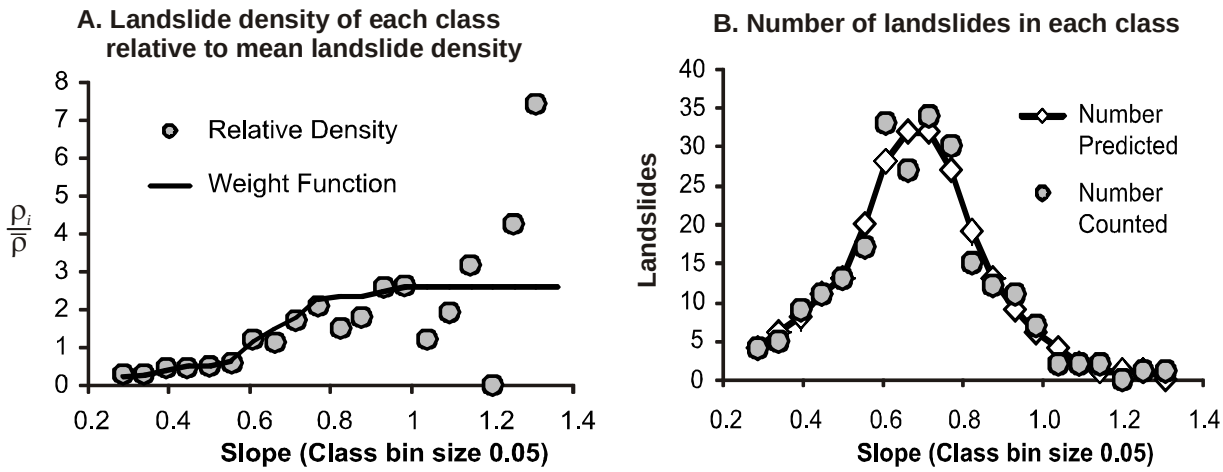

Figure 65. A. Relative landslide density for each slope class (density for the class divided by the mean density for all classes) and a topographic weighting function, Equation 3, fit to these values. B. The number of landslides counted in each class and predicted with the weight function shown in 2A.

A weighting term can be defined for any subset of DEM cells using Equation 3. In the example above, we defined this subset in terms of all cells (and associated landslides) falling within a specified gradient class. We can do the same for other measures of topographic form (e.g., convergence, drainage area, relief, distance to a stream, etc.). These factors are referred to here as topographic indices.

The appropriate index to use depends on the characteristic topography where landslides tend to occur and varies with landslide type (e.g., landslides triggered by rain infiltration versus those triggered by stream undercutting). Rainfall triggered landslides and associated debris flows form an important mechanism for delivery of sediment to streams in coastal Oregon (e.g., Dietrich and Dunne 1978; Robison, Mills et al. 1999). These landslides tend to initiate on steep slopes, commonly in areas of topographic convergence (i.e., hollows) (Reneau, Dietrich et al. 1990; Dunne 1998), although such landslides also occur on planar slopes (May 2002). Dependence of landslide initiation on topographic convergence may differ with storm characteristics; Wieczorek (1987), for example, found in the San Francisco Bay region that long-duration, moderate intensity storms triggered landslides on concave slopes with large drainage areas (i.e., in hollows), whereas short-duration, high-intensity storms triggered landslides on planar slopes with no drainage-area dependence. Thus topographic indices for shallow-rapid landsliding should include slope gradient and potentially some measure of topographic convergence and drainage area.

The relative performance of different indices may be evaluated by calculating weighting values (Equation 3) for all DEM cells within a study area and then, starting with the least-stable sites (highest weights) and progressing to the most stable, determining the proportion of area included as a function of the proportion of mapped landslide initiation sites (Figure 66). The index that captures the largest proportion of landslides with the smallest proportion of area best resolves topographic controls indicated by the landslide inventory and topographic data used. However, other factors should also be considered in assessing any index, such as the potential that storms with characteristics different from those that triggered the landslides used for calibration can initiate landslides in topographic locations other than those indicated by the calibrated model. For this study,

we provide results for two indices, one using both slope gradient and topographic convergence (that may be appropriate for longer-duration storms), and another using slope gradient alone (that may be more appropriate for high-intensity storms).

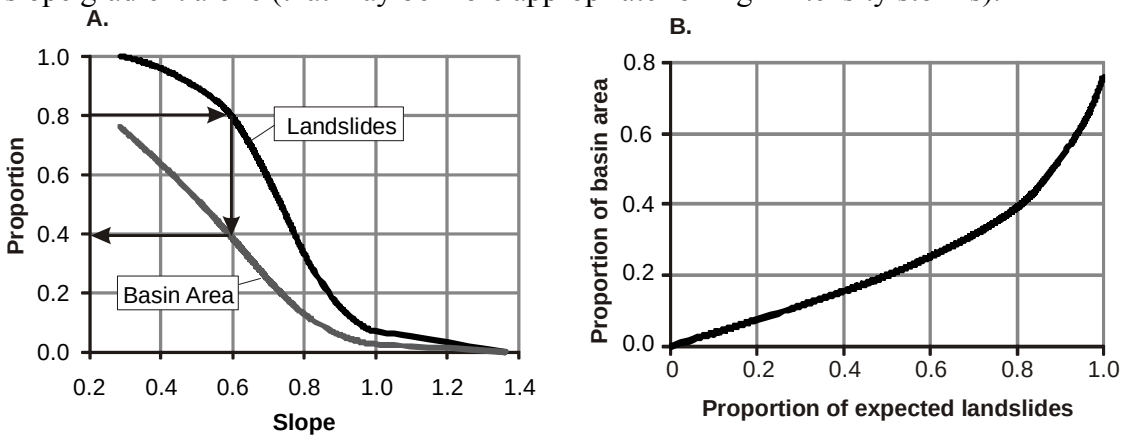

Figure 66. A. The proportion of mapped landslides and the proportion of ODF study-site area as a function of DEM-inferred slope. B. The curves in 3A translate to the proportion of basin area required to encompass a specified proportion of the mapped landslides, using slope as a measure of landslide susceptibility.

32.3.2 Model evaluation

Weighting terms (Equation 3) can be calibrated using a landslide inventory collected over a delineated area (note that Equation 3 requires both number of landslides and area). To evaluate the ability of the calibrated weighting terms to indicate landslide locations over some subset of the calibration area, or for some other area entirely, we can look at how the relative number of landslides predicted over specific classes of the topographic index compare to the proportion of landslides observed in each class. For example, using Equation 5 we can calculate the number of landslides *n* expected over slope gradients between 70% and 80%, and the number *N* expected over all slope gradients. The ratio *n*/*N* gives the proportion of all landslides expected in this gradient class; a prediction that can be compared to the actual proportion. For the jth class then, we define this proportion as

$$\frac{n_j}{N} = \frac{(\sum w)_{j^{th}\,class}}{(\sum w)_{all\,classes}} \tag{6}$$

The model is not used here to predict the actual number of landslides, only to predict where they are most likely to occur. Thus we can compare model predictions to observations, even though there may be differences in mean landslide density between data sets. In doing so, we must also account for the variability expected between data sets. If we were to collect landslide inventories for the same area at two different times, we expect some variability in the proportion of landslides found in each class (of the topographic index) because of the stochastic nature of landslide occurrence. The larger the number of landslides, the smaller this variability should be. Thus higher mean landslide densities and larger areas both result in lower expected variability. We can estimate this variability as follows (Miller and Burnett 2007). If we assume that landslide locations are independent of each other (that the location of one landslide has no effect on the location of other landslides), then we can approximate landslide locations as Poisson-

distributed variables and estimate the probability of having mapped a landslide in any DEM cell as a function of the landslide density calculated for that cell. We can use these probabilities to generate synthetic landslide inventories for the study area. For each DEM cell, we sample from a uniform distribution (between zero and one); if the sampled value is less than or equal to the probability calculated for the cell, we assign a landslide to the cell. We then determine the proportion of simulated landslides in each class of the topographic index. To estimate the range of variability to expect, we generate many synthetic inventories (e.g., 1000), each of which is consistent with the topographic controls indicated by the weighting terms. For each class, we find that these simulated proportions span a range of values, from which we determine specified confidence intervals, e.g., within what range do 90% of the predicted proportions fall? We can then see how observed values, calculated from landslide inventories, compare to the expected values and to the expected range of variability in each class. This provides a means to evaluate model performance, particularly when applying the model to sites outside of the calibration area.

It is also important to be cognizant of potential biases. For example, if smaller landslides, those harder to see under forest canopy, are associated with topographic locations that tend to differ from those for larger landslides, a landslide inventory obtained from air photo mapping may be biased towards the topographic locations indicative of larger landslides.

32.3.3 Translation to hazard classes

Here we define landslide hazard as a measure of relative susceptibility to landslide initiation. We are interested in differentiating areas where many landslides will occur from areas where few or none will occur, and in quantifying differences among sites. In this context, one strategy is to define hazard level in terms of the expected proportion of all landslides encompassed within a specified area. For a given DEM (or portion of a DEM), we first rank cells in order of decreasing weight value (increasing stability). Then the proportion P of expected landslides with weight values greater than or equal to W is given by

$$P_W = \frac{(\sum w)\,|_{w=w_{MAX}}^{W}}{(\sum w)\,|_{w=w_{MAX}}^{0}} \tag{7}$$

where w_{MAX} is the largest weight value for the DEM and the sums proceed along the ranked list from largest to smaller values. (Likewise, the number of cells with weight values greater than or equal to W divided by the total number of cells in the DEM of the study area gives the proportion of area with weights greater than or equal to W.) Plotting P_W as a function of W (or topographic index), from $W = 0$ to w_{MAX}, gives a curve indicating the weight value required to encompass any specified proportion of all expected landslides (Figure 67). Correspondingly, each DEM cell can then be assigned a value (between zero and one) indicating the proportion of all expected landslides with weight values greater than or equal to that of the cell. Specified proportions can now be set to define hazard zones. For example, Figure 67 shows hazard zones defined to capture 50%, 90%, and 100% of all expected landslides.

32.3.4 Data and results for the Wilson River Basin

Field-based landslide inventories collected by the Oregon Department of Forestry in the 1996 storm study (Robison, Mills et al. 1999) were used to calibrate topographic weighting terms (Miller and Burnett 2007). For this watershed analysis, two DEM-derived topographic indices were used: slope gradient S, calculated from a polynomial fit to the elevations of a DEM cell and its eight adjacent neighbors (Zevenbergen and Thorne 1987), and a function I using slope and the local specific contributing area, A_L/b, which provides a measure of topographic convergence:

$$I = S\frac{A_L}{b} \tag{8}$$

For any DEM cell, A_L specifies the number of adjacent cells that drain into it and provides a measure of local contributing area; approximately that derived from within 15 m of each DEM point. We use the D∞ flow-direction algorithm (Tarboton 1997), which estimates the proportion of each cell draining into its neighbors; thus A_L can vary continuously from zero (a local peak) to eight (a local pit) and includes non-integer values. Dividing drainage area by b, the width of flow in cell widths measured perpendicular to flow direction for water draining from the cell, gives specific drainage area. This width is estimated by projecting flow direction against the cell edge: convergent topography yields a b value less than one, planar slopes have a b value of one, and divergent topography has a b value greater than one.

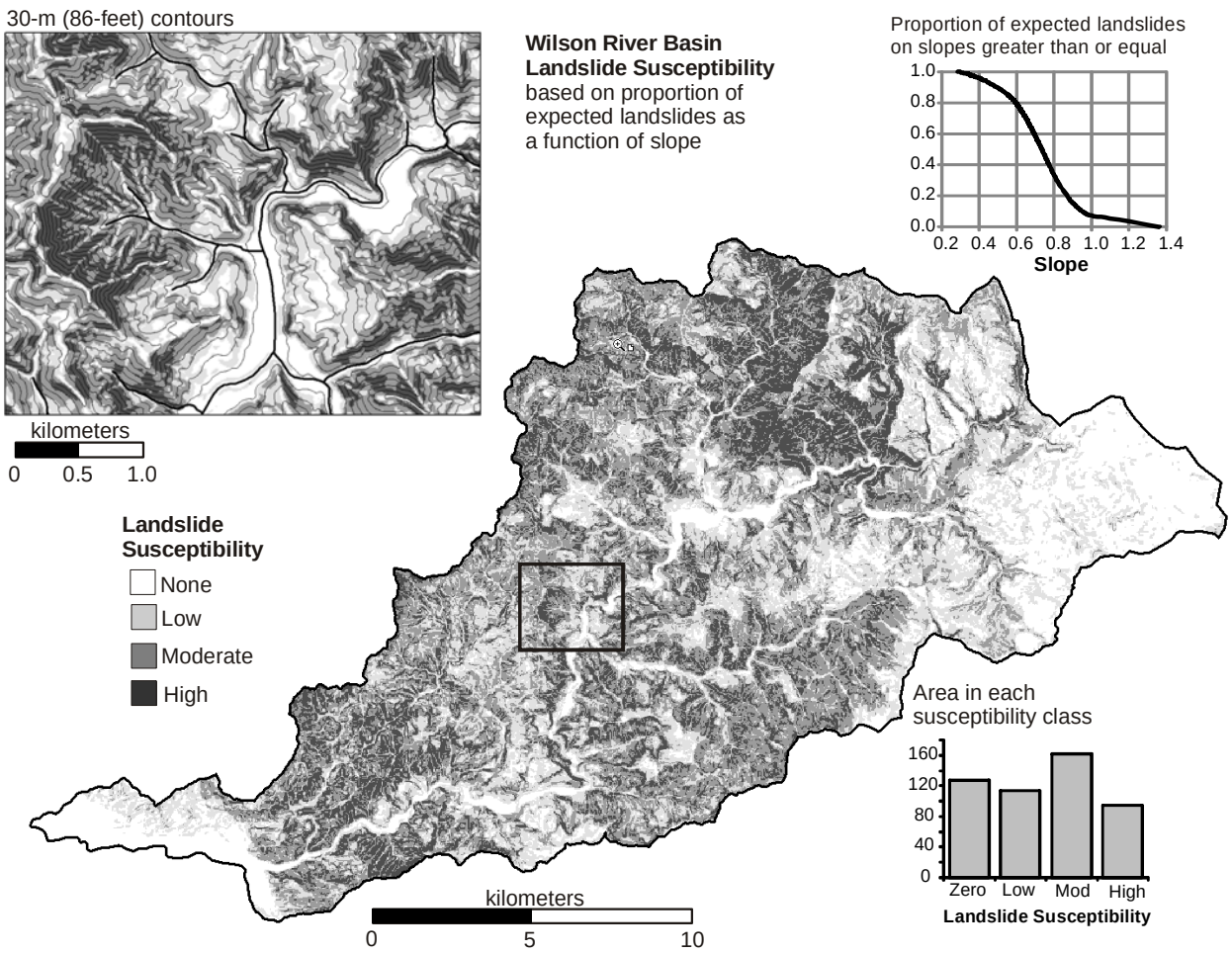

Figure 67. Landslide susceptibility, defined to capture a specified proportion of expected landslide initiation sites ranked from the most to least susceptible. In this example, the High category is defined to encompass the least stable sites to capture 50% of all expected landslides, the High + Moderate categories will capture 90% of all expected landslides, and the Low category encompasses the least susceptible sites required to capture the remaining 10% of expected landslide initiation sites. These maps are plotted from the prop_slope GIS grid; the number of categories and the levels at which they are defined can be readily changed.

Mapped initiation points for each upland, non-road-related landslide (Robison, Mills et al. 1999) in the Mapleton, Scottsburg, Elk Creek, Dallas, and Tillamook study sites were overlain on index values calculated from 10-m DEMs and associated with the highest index value (least stable cell) within a 15-m radius of the digitized location. This procedure was intended to account for the expected level of imprecision in the mapping and digitizing of landslide locations. On a 1:24,000-scale base map, 15 m corresponds to a little more than half a millimeter, about the width of a pencil line. Index values for all landslides were ranked and divided into equally spaced classes, spanning the smallest to the largest index values found for landslides in the inventory. The number of landslides and the area of the study sites encompassed in each class were calculated to define weighting values (Equation 3). To provide a smooth, continuous functional form for *w*, a piecewise linear spline was defined to maximize agreement with the number of landslides counted in each class while also maintaining a relatively smooth curve. The resulting weight functions for both indices are shown in Figure 68.

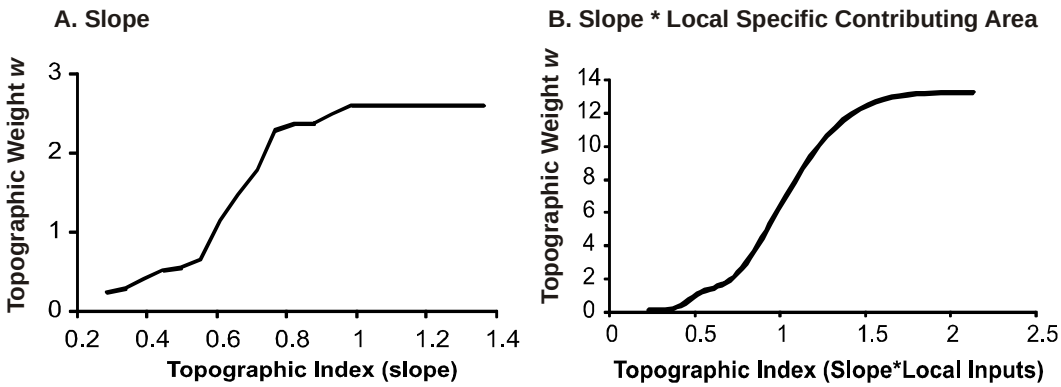

Figure 68. Topographic weighting terms calibrated to ODF 1996-Storm Study field sites. A. For a slope-based topographic index. B. For a slope*local specific contributing area (Equation 8) based index. Note the change in vertical scale between the two graphs.

For the combined data from the five sites used for calibration, the two indices yield somewhat different curves for the area required to encompass a given proportion of surveyed landslides, with the index using both slope and topographic convergence better resolving topographic controls on landslide location (Figure 69a). The same applies for curves calculated for the Wilson River watershed (Figure 69b).

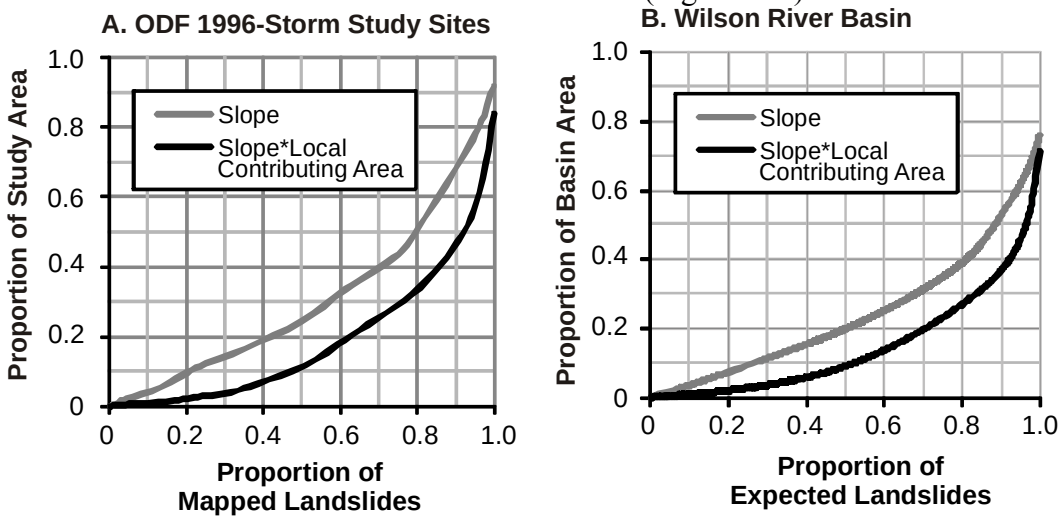

Figure 69. The proportion of basin area required to encompass specified proportions of landslide initiation sites based on the two weighting functions in Figure 5 for A. the ODF study sites and B. for the Wilson River Basin.

How well does a weight function calibrated to all five ODF study sites, which are predominately underlain by sandstones (versus the basaltic igneous rocks prevalent in the Wilson basin), work for the Wilson? Results from the Tillamook site provide some insight. For the Tillamook site, Figure 70 shows the cumulative proportion of expected and observed landslides with index values greater than or equal to that specified along the X axis, along with 90% confidence intervals. For a given index value, we tend to overestimate the proportion of landslides using slope, although the empirical curve falls within the modeled 90% confidence interval, and to under estimate the proportion using slope and curvature, with observed proportions falling outside the 90% confidence intervals over a portion of the range. This result suggests that slope may be a better choice for the Wilson.

Why do results at Tillamook differ from the average over all five ODF study sites? Two hypotheses come to mind: topographic controls in basaltic bedrock differ from those in sandstone, or storm characteristics at Tillamook were different than those at the other sites, which were all further south. Without further data to evaluate these hypotheses, we are reluctant to define a weight function using the Tillamook data alone. The smaller data set would entail greater uncertainty in the resulting weight function, and may be missing storm effects manifest in data from the other sites.

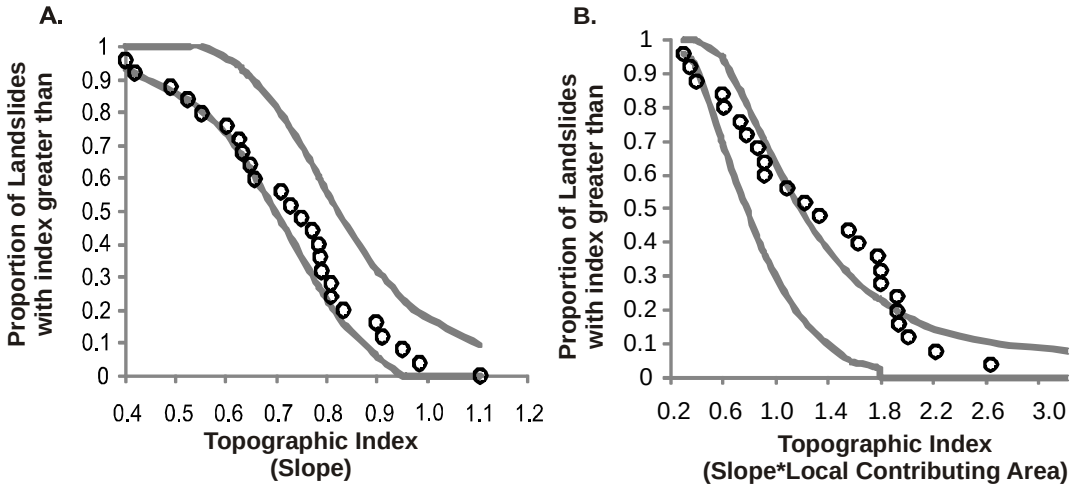

Figure 70. Predicted range, using the weighting functions calibrated to the ODF 1996-storm study sites, and observed values for landslides in the ODF 1996-Storm Tillamook study site. A. Slope-based topographic index, B. Slope * Local Specific Contributing Area index.

32.3.5 Hazard ratings for landslide initiation

Each cell in the DEM of the Wilson basin has a calculated index value and corresponding topographic weighting term. Curves such as that in Figure 67 were used to assign to each cell the proportion of landslides having weights (index values) greater than or equal to that of the cell. The resulting grid files (prop_slope and prop_gep for the two topographic indices) can be used to delineate hazard zones defined to encompass a given proportion of all expected landslide sites. The example shown in Figure 67 has hazard levels defined to include 50%, 90%, and 100% of all expected landslides. These levels are presented only as examples; different values can be specified and new maps plotted in ArcMap using these grids.

32.4 Debris-flow runout

32.4.1 Topographic factors

The extent of debris flow runout, and the tendency for a debris flow to erode or deposit material along the flow path, have been observed to correlate with three primary topographic attributes: slope gradient, the degree of topographic confinement, and changes in flow direction at tributary junctions (Benda and Cundy 1990; Fannin and Rollerson 1993; Robison, Mills et al. 1999). These attributes have been used to define simple field- and map-based protocols for identifying areas subject to debris-flow scour and deposition (Benda and Cundy, 1990; Oregon Board of Forestry, 2001). To expand such analyses to a GIS-based tool for regional assessment of debris-flow potential, Miller

and Burnett (2007) derived an empirically calibrated model for calculating probability for debris-flow runout using these three topographic attributes as inferred from a 10-m DEM. This model calculates a probability for a debris flow originating in any DEM cell to travel down slope, cell to cell, as a function of these topographic attributes along the cumulative flow path.

32.4.2 Model calibration and evaluation

The model was calibrated using field-mapped runout extents from the ODF 1996-storm study site near Mapleton (Robeson et al., 1999), underlain by Tyee sandstones (Walker and MacLeod 1991). We now intend to use it for the Wilson River Basin, underlain by basaltic rocks. How well does the model calibration translate to this area? Miller and Burnett (2007b) examined this issue in part by applying the model in the Tillamook study area, which is wholly contained in the Wilson Basin. This evaluation was based on the proportion of channel length predicted and observed to have contained mapped evidence of debris flows. The model worked well for smaller (< 4rd-order) channels, but under predicted the extent of channel length with mapped debris flow effects for larger channels (Figure 71). Miller and Burnett (2007) hypothesize that this difference between the two study sites arises because of differences in mean channel size (drainage area) and gradient: channels at the Tillamook site tend to be steeper and larger than channels at the Mapleton site. Larger, steeper channels have greater stream power and a greater tendency to rapidly erode debris-flow deposited material (Benda, Veldhuisen et al. 2003), thereby forming debris-laden floods.

Nevertheless, our interest here is in the smaller channels. Headwater channels flowing to fish-bearing streams are, almost exclusively, third and lower-order (as determined from the DEM-traced channel network using the same criteria as used by Miller and Burnett, (2007), Figure 72). Delivery to fish-bearing streams solely involves areas for which the model worked well.

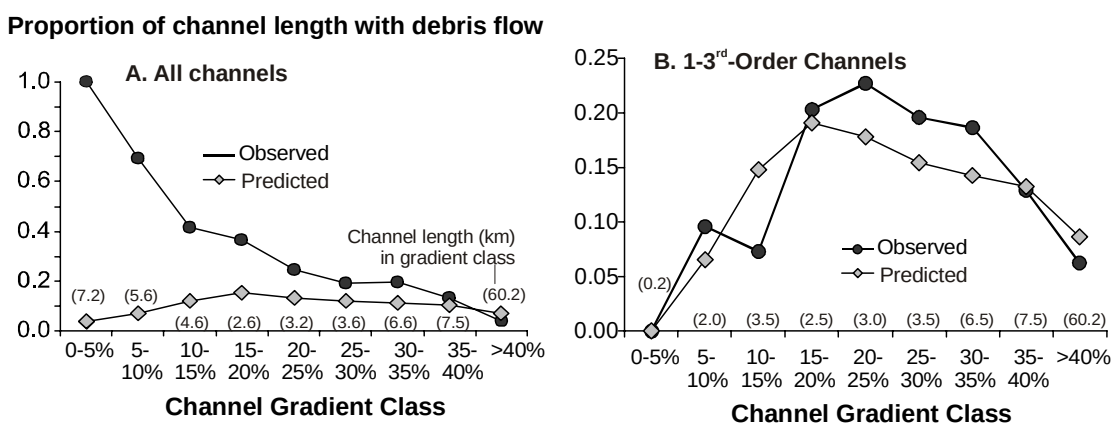

Figure 71. The proportion of channel length in each channel-gradient class predicted and observed to contain evidence of debris (torrent) passage for the Tillamook study site, for A. all channels (97% of low-gradient, <5%, channels were mapped as having high debris-torrent impacts). and B. only 1st – 3rd-order channels.

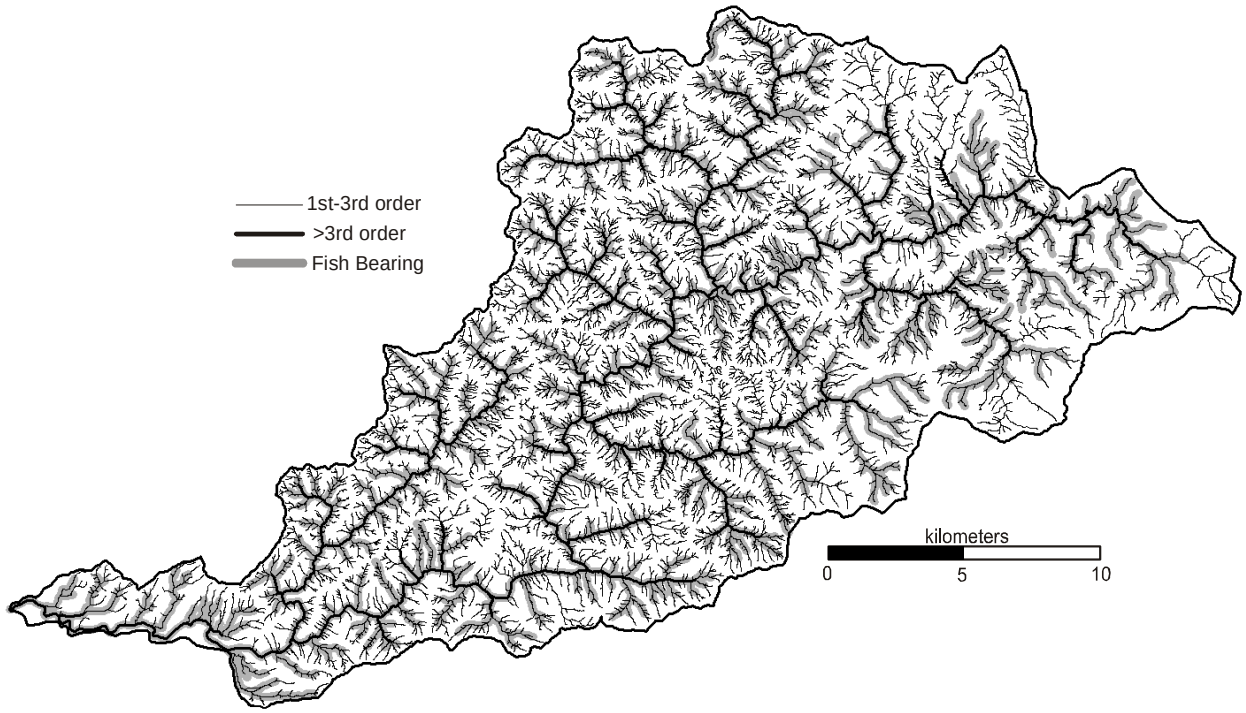

Figure 72. Stream order versus Type F (fish-bearing) channels. Type F streams extend into 3rd-order channels.

32.4.3 Delivery probability

For each DEM cell having a greater-than-zero topographic weighting for landslide initiation, the model traces the down slope flow path until it intersects a fish-bearing stream. The calculated probability for a debris flow to reach each downslope cell decreases monotonically as a function of gradient, topographic confinement, and channel-junction angles along the flow path. The probability, referred to as the probability for delivery P_D, calculated at the point where the flow path intersects a fish-bearing stream is then assigned to the source cell. This is repeated for all source cells. The resulting raster file provides a map of potential for debris-flow delivery from every cell in the basin, with values that vary from zero to one (Figure 73).

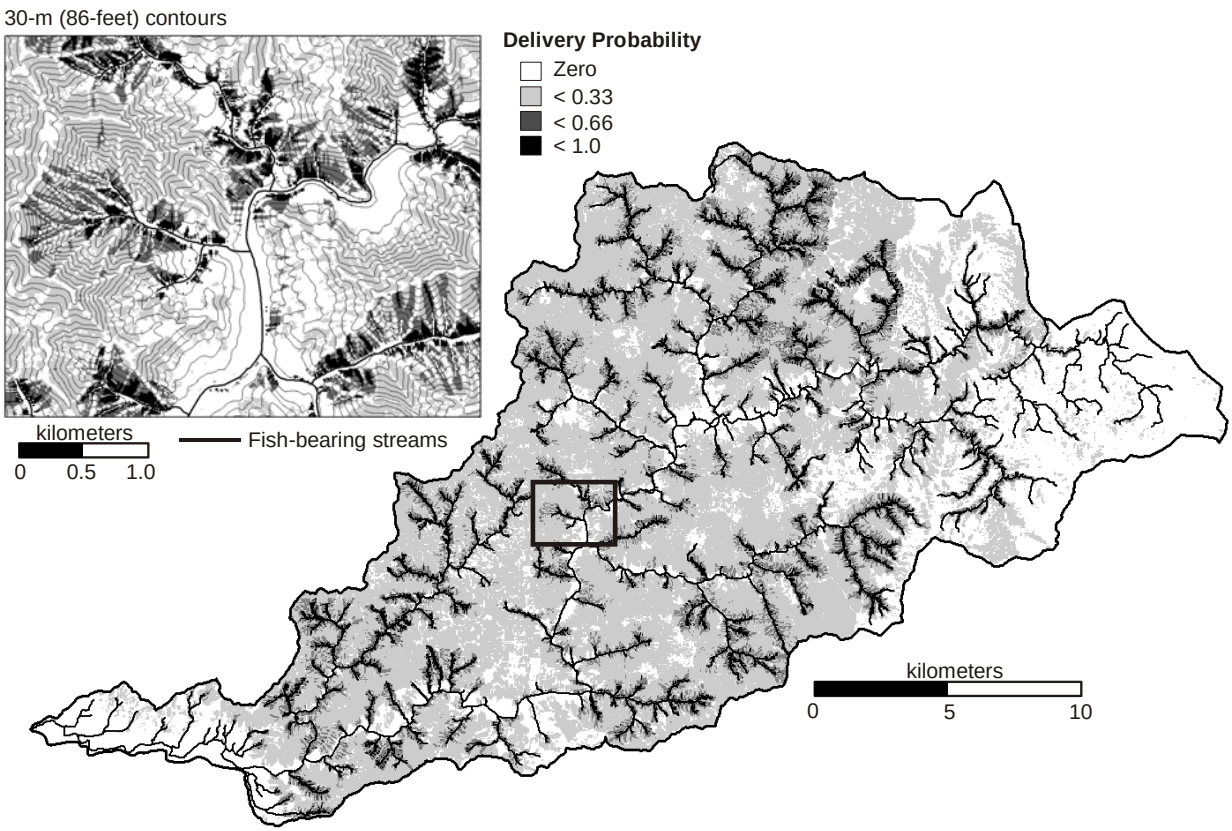

Figure 73. Probability of debris-flow delivery from each DEM cell to a Type F (fish-bearing) stream.

32.4.4 Incorporation of delivery probability into hazard ratings

The probability for delivery can be used with the mean landslide density and topographic weighting to calculate the expected number of landslides that delivered to fish-bearing streams. Following from Equation 5,

$$N = \overline{\rho} a_c \sum P_{D_i} w_i \tag{9}$$

where P_{Di} is the delivery probability for the ith cell. We can now follow the same strategy used to define hazard ratings for landslide initiation: we define hazard level in terms of the expected proportion of all landslides that generate debris flows that deliver to fish-bearing streams encompassed within a specified area. We first rank cells in order of decreasing value for the product of delivery probability and topographic weighting ($P_D w$). Then by adapting Equation 7, the proportion of landslides (that deliver) with $P_D w$ values greater than or equal to a specified value X is given by

$$P_{DELIVER} = \frac{(\sum P_D w)|_{P_D w = P_D w_{MAX}}^{X}}{(\sum P_D w)|_{P_D w = P_D w_{MAX}}^{0}} \tag{10}$$

As before, we can now identify the area required to encompass a given proportion of the expected landslides that deliver to fish-bearing streams, starting with those most likely to occur. This provides a quantifiable definition of hazard that includes both susceptibility

to landslide initiation, via the topographic weighting term, and the potential for delivery to the resource of interest -- fish-bearing streams.

Equations 9 and 10 incorporate the potential for debris-flow delivery into a definition of hazard, but it is prudent to examine hazards posed from other perspectives as well. For example, the magnitude of debris-flow effects might be considered, in part, proportional to the runout length. Damage to headwater channels is proportional to the length traversed and the volumes carried to and deposited in fish-bearing streams and riparian zones are generally larger for longer-runout debris flows (May, 2003). An assessment of hazard based solely on the potential for occurrence and delivery does not differentiate between large and small debris flows; in fact, source areas for some long-runout debris flows will be assigned a low hazard rating because of a low probability for delivery. Low probability does not imply no such debris flows, only that we expect a lower number of long-runout debris flows. This is consistent with empirical observations: field inventories indicate a skewed distribution of runout lengths, with a large number of relatively short-runout debris flows and few long ones (Robison, Mills et al. 1999; May 2002; Lancaster, Hayes et al. 2003). However, a single, long-runout debris flow may have impacts equal to or greater than many smaller, short-runout debris flows. To identify the source areas that generate the largest cumulative debris-flow impacts, we may want to consider both the relative number of debris-flow occurrences, which we gauge using $P_D w$, and the runout length. In the context of landslide density, we used $\overline{\rho} a_c \sum P_{D_i} w_i$ (Equation 9) to estimate the expected number of landslides that deliver to fish-bearing streams. Likewise, we can estimate the expected cumulative runout length L to fish-bearing streams as

$$L = \overline{\rho} a_c \sum R_i P_{D_i} w_i \tag{11}$$

where R_i is the runout length from the source cell to the fish-bearing stream for the ith debris flow. The product $RP_D w$ provides a measure of the potential impacts posed by each source cell that incorporates susceptibility, delivery, and runout length. An alternative measure of debris-flow hazard is to rank cells by this product, and then to sum $P_D W$ (to get the expected number of landslides that deliver) starting with the largest $RP_D w$ values and progressing to the smallest. Using Equation 10, but with the order of the sums based on $RP_D w$, we can identify the proportion of landslides with $RP_D w$ values greater than or equal to a specified value. Then each DEM cell can be assigned the proportion associated with its $RP_D w$ value. The resulting grid can be used to delineate areas required to encompass a specified proportion of all expected landslides that deliver to fish-bearing streams, starting with those having the largest $RP_D w$ values. This way, the highest hazard is assigned to source areas with the greatest cumulative debris-flow impacts, based on the cumulative runout length for the number of debris flows expected from each zone.

32.4.5 Identification of debris-flow-prone Type N channels

Our interest here is to identify Type N (non-fish-bearing) streams that have a high probability for debris-flow delivery of wood to Type F (fish-bearing) streams. Any Type N stream can potentially receive debris flows from a large number of landslide source areas. The potential that a debris flow was triggered upslope and that it continued through the Type N stream to a Type F stream depends on the number of upslope source areas,

the landslide susceptibility of those source areas, and the delivery probability from every potential source. To characterize the potential that any Type N stream is traversed by a debris flow that continues to a Type F stream, we go through the DEM cell by cell, and for each cell calculate the probability P_{ID} for both landslide initiation and delivery to a Type F stream. This probability is then applied to each cell along the flow path. To account for multiple debris-flow sources, for each cell along a flow path we calculate:

$$P_T = 1 - \prod (1 - P_{ID_i}) \tag{12}$$

where P_T is the probability of debris-flow traversal from a source area upslope, the product is performed over all upslope cells, and P_{IDi} is the probability for debris-flow initiation and delivery to a Type F stream for the ith upslope cell. A P_T value is calculated for every DEM cell. Following Burnett and Miller (2007), we use the P_T values to estimate the total stream length potentially traversed by debris flows:

$$L_{DF} = \sum P_{T_i} l_i \tag{13}$$

where P_{Ti} and l_i are the P_T value and flow length through the ith cell. If the sum is performed starting with the largest and progressing to the smallest P_T values, then the proportion of total debris-flow track length can be calculated as a function of P_T. As with Equation 10, the proportion of total debris-flow track length (P_{DF}) with a P_T value greater than or equal to X is given by

$$P_{DF}(X) = \frac{(\sum P_T\ l)|_{P_T=P_{TMAX}}^{X}}{(\sum P_T\ l)|_{P_T=P_{TMAX}}^{0}} \tag{14}$$

A curve giving P_{DF} as a function of P_T shows the P_T value required to encompass any specified proportion of the expected debris-flow-track length associated with a large storm (Figure 11). Each cell of the DEM has an associated P_T value, so we can now classify each cell in terms of the proportion of expected debris-flow track length having P_T values greater than or equal to that of the cell. Because a large number of potential debris-flow sources can flow into a single low-order channel, a large proportion (about 70%) of the potential debris-flow track length is concentrated in the Type N channels, with the remaining track length in areas upslope. Type N channels can now be characterized in terms of the potential that they are traversed by debris flows that travel to a Type F stream. Figure 11 shows the channels expected to contain 25%, 50%, and 75% of the expected debris-flow-track length.

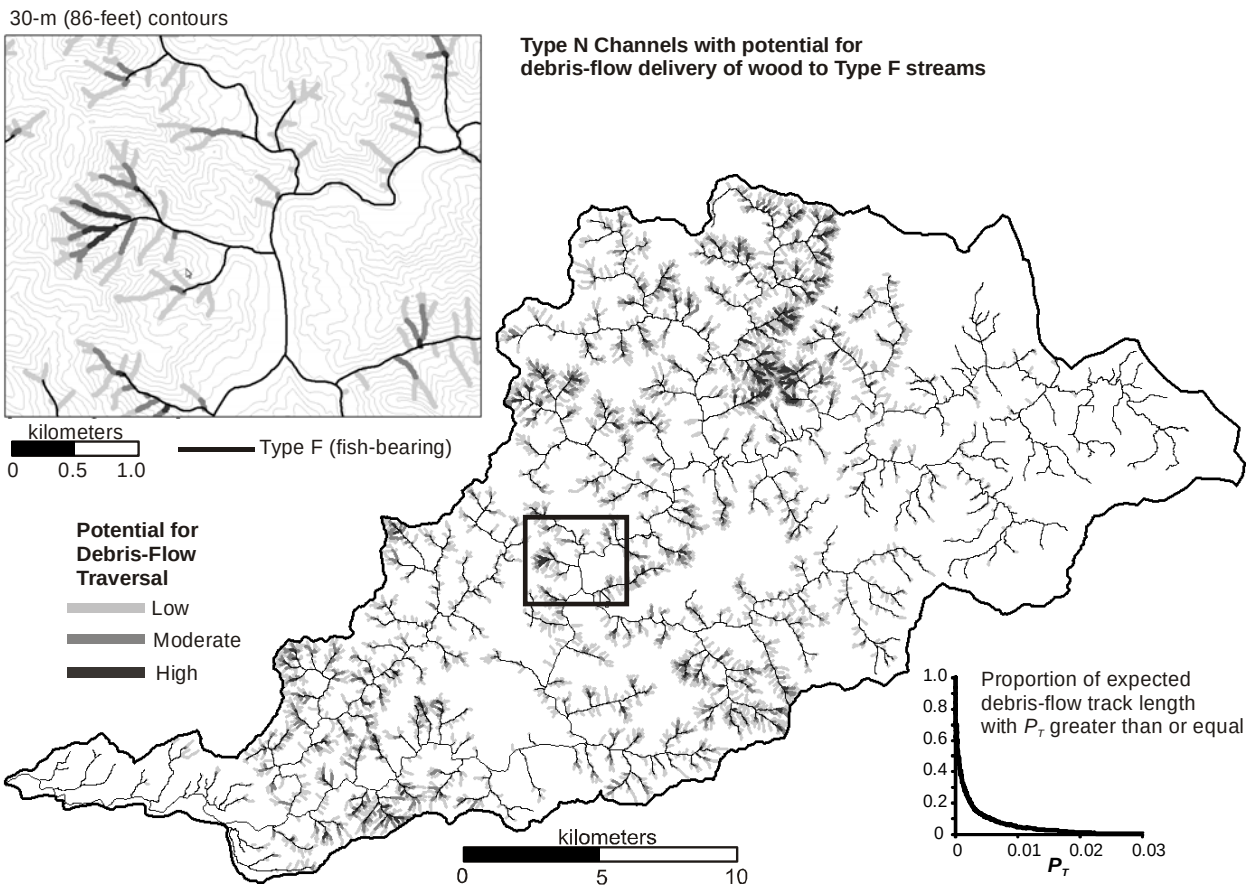

Figure 74. Debris-flow-prone Type N (non-fish-bearing) channels. Categories for susceptibility to debris-flow traversal are defined to encompass specified proportions of the expected debris-flow track length. Channels with a High rating encompass 25% of the expected track length; together channels with a High and Moderate rating encompass 50% of the expected track length, and the High, Moderate, and Low category channels encompass 75% of the expected debris-flow track length. Beyond this level, expected debris flow tracks extend primarily to landslide source areas upslope of defined channels.

32.4.6 Debris-Flow-Prone Type F Streams

To evaluate the potential for debris-flow deposition in fish-bearing streams, we must account for every potential upstream debris-flow source. Following Miller and Burnett (2007), we track the DEM-inferred downslope flow path from every DEM cell having a greater-than-zero landslide susceptibility. We use $(P_I P_R)_{ij}$ to refer to the probability that a debris flow initiating in cell *i* reaches cell *j* along the travel path, where P_I is the initiation probability and P_R is the probability that the debris flow runs out to cell *j*. Both P_I and P_R are calculated as functions of DEM-derived topographic attributes (Miller and Burnett 2007; Miller and Burnett 2007). For every cell *j* containing a fish-bearing channel, the probability P_{Fj} that a debris flow from any upslope source reaches the cell is calculated as

$$P_{F_j} = 1 - \prod_i (1 - (P_I P_R)_{ij}) \tag{15}$$

with the product performed over all upslope pixels. This probability provides a relative ranking of debris-flow susceptibility for all fish-bearing channels.

To assign relative hazard levels to each reach, we again consider channels in terms of the proportion of channel length affected. An estimate of the length L_F of Type F channels affected by debris flows during a large storm is calculated as $L_F = \Sigma(P_{Fj} l_j)$, with the sum performed over all Type-F channel reaches. If reaches are ranked from large to low P_F values prior to performing this sum, we can then estimate the proportion of debris-flow-affected channel length as a function of P_F using Equation 14, but with P_T replaced by P_F. Actual debris-flow track length differs from storm to storm and from basin to basin; this exercise estimates how that track length is distributed across the channel network to identify those channels most likely to be affected. The resulting curve differs from basin to basin; an area with a large number of reaches with a low debris-flow probability will have a large proportion of the debris-flow-affected channels occurring in low-probability reaches. The curve for the Wilson Basin is shown in Figure 75 below:

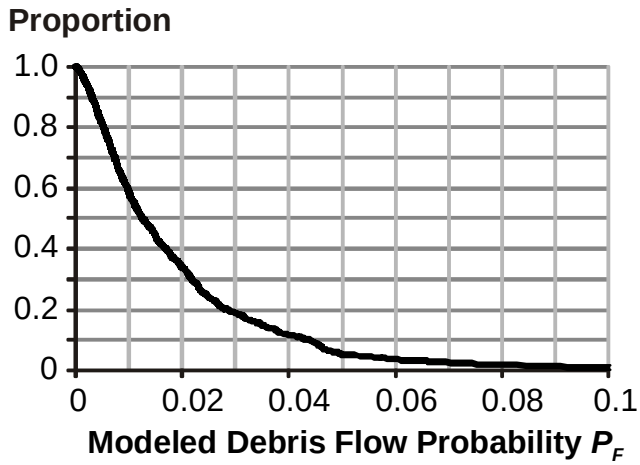

Figure 75. Proportion of debris-flow-prone, Type F channel length with P_F values greater than or equal to that on the X axis.

This curve can be used to define hazard levels to include a specified proportion of the expected debris flow occurrences. For example, to include 25% of the expected debris-flow-affected channel length in each level, a High hazard corresponds to $P_F > 0.025$, Moderate High to $0.025 > P_F > 0.013$, Moderate Low to $0.013 > P_F > 0.006$, and Low to $P_F < 0.006$.

32.5 References

Beechie, T. J., G. Pess, et al. (2000). "Modeling recovery rates and pathways for woody debris recruitment in northwestern Washington streams." North American Journal of Fisheries Management **20**: 436-452.

Beechie, T. J. and T. H. Sibley (1997). "Relationships between channel characteristics, woody debris, and fish habitat in northwestern Washington streams." Transactions of the American Fisheries Society **126**: 217-229.

Benda, L. E. (1990). "The influence of debris flows on channels and valley floors in the Oregon Coast Range, U.S.A." Earth Surface Processes and Landforms **15**: 457-466.

Benda, L. E., K. Andras, et al. (2004). "Confluence effects in rivers: Interactions of basin scale, network geometry, and disturbance regimes." Water Resources Research **40**: W05402.

Benda, L. E. and T. W. Cundy (1990). "Predicting deposition of debris flows in mountain channels." Canadian Geotechnical Journal **27**: 409-417.

Benda, L. E., C. Veldhuisen, et al. (2003). "Debris flows as agents of morphological heterogeneity at low-order confluences, Olympic Mountains, Washington." Geological Society of America Bulletin **115**(9): 1110-1121.

Bigelow, P. E., L. E. Benda, et al. (2007). "On debris flows, river networks, and the spatial structure of channel morphology." Forest Science **53**(2): 220-238.

Bilby, R. E., J. T. Heffner, et al. (1999). "Effects of immersion in water on deterioration of wood from five species of trees used for habitat enhancement projects." North American Journal of Fisheries Management **19**: 687-695.

Burnett, K. M. and D. J. Miller (2007). "Streamside policies for headwater channels: an example considering debris flows in the Oregon Coastal Province." Forest Science **53**(2): 239-253.

Clarke, S. E., K. M. Burnett, et al. (in press). "Modeling streams and hydrogeomorphic attributes in Oregon from digital and field data." Journal of the American Water Resources Association.

Dietrich, W. E. and T. Dunne (1978). "Sediment budget for a small catchment in mountainous terrain." Zietshrift für Geomorphologie **Suppl. Bd. 29**: 191-206.

Dunne, T. (1998). "Critical data requirements for prediction of erosion and sedimentation in mountain drainage basins." Journal of the American Water Resources Association **34**(4): 795-808.

ESRI (1998). ESRI Shapefile Technical Description, An ESRI White Paper, Environmental Systems Research Institute, Inc.**:** 34.

Everest, F. H. and W. R. Meehan (1981). "Forest management and anadromous fish habitat productivity." Transactions of the North American Wildlife and Natural Resources Conference **46**: 521-530.

Fannin, R. J. and T. P. Rollerson (1993). "Debris flows: some physical characteristics and behavior." Canadian Geotechnical Journal **30**(1): 71-81.

Grant, G. G. and F. J. Swanson (1995). Morphology and processes of valley floors in mountain streams, Western Cascades, Oregon. Natural and Anthropogenic Influences in Fluvial Geomorphology, Geophysical Monograph 89. J. E. Costa, A. J. Miller, K. W. Potter and P. R. Wilcock. Washington, D.C., American Geophysical Union**:** 83-101.

Hogan, D. L., S. A. Bird, et al. (1998). Stream channel morphology and recovery processes. Carnation Creek and Queen Charlotte Islands Fish/Forestry Workshop: Applying 20 Years of Coast Research to Management Solutions. Land management handbook 41. D. L. Hogan, P. J. Tschaplinski and S. Chatwin. Victoria, B.C., Crown Publications, Inc.**:** 77-96.

Hyatt, T. L. and R. J. Naiman (2001). "The residence time of large woody debris in the Queets River, Washington, USA." Ecological Applications **11**(1): 191-202.

Lancaster, S. T. and G. E. Grant (2006). "Debris dams and the relief of headwater streams." Geomorphology: 14.

Lancaster, S. T., S. K. Hayes, et al. (2003). "Effects of wood on debris flow runout in small mountain watersheds." Water Resources Research **39**(6): doi:10.1029/2001WR001227.

May, C. L. (2002). "Debris flows through different forest age classes in the central Oregon Coast Range." Journal of the American Water Resources Association **38**(4): 1-17.

May, C. L. and R. E. Gresswell (2003). "Processes and rates of sediment and wood accumulation in headwater streams of the Oregon Coast Range, USA." Earth Surface Processes and Landforms **28**(4): 409-424.

May, C. L. and R. E. Gresswell (2004). "Spatial and temporal patterns of debris-flow deposition in the Oregon Coast Range, USA." Geomorphology **57**: 135-149.

Miller, D. J. and L. E. Benda (2000). "Effects of punctuated sediment supply on valley-floor landforms and sediment transport." Geological Society of America Bulletin **112**(12): 1814-1824.

Miller, D. J. and K. M. Burnett (2007). "Effects of forest cover, topography, and sampling extent on the measured density of shallow, translational landslides." Water Resources Research **43**(W03433).

Miller, D. J. and K. M. Burnett (2007). "A probabilistic model of debris-flow delivery to stream channels, demonstrated for the Coast Range of Oregon, USA." Geomorphology.

Reneau, S. L., W. E. Dietrich, et al. (1990). "Late Quaternary history of colluvial deposition and erosion in hollows, central California Coast Ranges." Geological Society of America Bulletin **102**: 969-982.

Roberts, R. G. and M. Church (1986). "The sediment budget in severely disturbed watersheds, Queen Charlotte Ranges, British Columbia." Canadian Journal of Forest Research **16**: 1092-1106.

Robison, G. E., K. A. Mills, et al. (1999). Storm impacts and landslides of 1996: final report. Salem, OR, Oregon Department of Forestry**:** 145.

Sobota, D. J., S. V. Gregory, et al. (2006). "Riparian tree fall directionality and modeling large wood recruitment to streams." Canadian Journal of Forest Research **36**: 1243-1254.

Tarboton, D. G. (1997). "A new method for the determination of flow directions and upslope areas in grid digital elevation models." Water Resources Research **33**(2): 309-319.

Walker, G. W. and N. S. MacLeod (1991). Oregon Geology. Reston, VA, U.S. Department of the Interior, Geological Survey.

Wieczorek, G. F. (1987). Effect of rainfall intensity and duration on debris flows in central Santa Cruz Mountains, California. Debris Flows / Avalanches: Process, Recognition, and Mitigation. J. E. Costa and G. F. Wieczorek. Boulder, CO, The Geological Society of America. **7:** 93-104.

Wohl, E. E. and P. P. Pearthree (1991). "Debris flows as geomorphic agents in the Huachuca Mountains of southeastern Arizona." Geomorphology **4**: 273-292.

Zevenbergen, L. W. and C. R. Thorne (1987). "Quantitative analysis of land surface topography." Earth Surface Processes and Landforms **12**: 47-56.

33 Appendix U – Major Vegetation Classifications Used in the Vegetation Analysis

Table 1. Major Vegetation Classifications. The consolidated classifications used for landscape-level vegetation analyses, derived from FPS codes.

Vegetation Code	Major Type	Size Description	DBH Range	Density Description
FC1H	Conifer	Early and Mid-Seral	0 - 8 in. DBH	High/ Homogeneous Density
FC1L	Conifer	Early and Mid-Seral	0 - 8 in. DBH	Low Density/ Patchy
FC1M	Conifer	Early and Mid-Seral	0 - 8 in. DBH	Medium Density
FC2H	Conifer	Late Seral: Small	8 - 14 in. DBH	High/ Homogeneous Density
FC2L	Conifer	Late Seral: Small	8 - 14 in. DBH	Low Density/ Patchy
FC2M	Conifer	Late Seral: Small	8 - 14 in. DBH	Medium Density
FC3H	Conifer	Late Seral: Medium	14 - 20 in. DBH	High/ Homogeneous Density
FC3L	Conifer	Late Seral: Medium	14 - 20 in. DBH	Low Density/ Patchy
FC3M	Conifer	Late Seral: Medium	14 - 20 in. DBH	Medium Density
FC4H	Conifer	Late Seral: Large	20 - 30 in. DBH	High/ Homogeneous Density
FC4L	Conifer	Late Seral: Large	20 - 30 in. DBH	Low Density/ Patchy
FC4M	Conifer	Late Seral: Large	20 - 30 in. DBH	Medium Density
FC5H	Conifer	OFS Candidate	>30 in. DBH	High/ Homogeneous Density
FC5L	Conifer	OFS Candidate	>30 in. DBH	Low Density/ Patchy
FC5M	Conifer	OFS Candidate	>30 in. DBH	Medium Density
FH1H	Hardwood	Early and Mid-Seral	0 - 8 in. DBH	High/ Homogeneous Density
FH1L	Hardwood	Early and Mid-Seral	0 - 8 in. DBH	Low Density/ Patchy
FH1M	Hardwood	Early and Mid-Seral	0 - 8 in. DBH	Medium Density
FH2H	Hardwood	Late Seral: Small	8 - 14 in. DBH	High/ Homogeneous Density
FH2L	Hardwood	Late Seral: Small	8 - 14 in. DBH	Low Density/ Patchy
FH2M	Hardwood	Late Seral: Small	8 - 14 in. DBH	Medium Density
FH3H	Hardwood	Late Seral: Medium	14 - 20 in. DBH	High/ Homogeneous Density
FH3L	Hardwood	Late Seral: Medium	14 - 20 in. DBH	Low Density/ Patchy
FH3M	Hardwood	Late Seral: Medium	14 - 20 in. DBH	Medium Density
FH4H	Hardwood	Late Seral: Large	20 - 30 in. DBH	High/ Homogeneous Density
FH4L	Hardwood	Late Seral: Large	20 - 30 in. DBH	Low Density/ Patchy
FH4M	Hardwood	Late Seral: Large	20 - 30 in. DBH	Medium Density
FH5H	Hardwood	OFS Candidate	>30 in. DBH	High/ Homogeneous Density
FH5L	Hardwood	OFS Candidate	>30 in. DBH	Low Density/ Patchy
FH5M	Hardwood	OFS Candidate	>30 in. DBH	Medium Density
FM1H	Mixed	Early and Mid-Seral	0 - 8 in. DBH	High/ Homogeneous Density
FM1L	Mixed	Early and Mid-Seral	0 - 8 in. DBH	Low Density/ Patchy
FM1M	Mixed	Early and Mid-Seral	0 - 8 in. DBH	Medium Density
FM2H	Mixed	Late Seral: Small	8 - 14 in. DBH	High/ Homogeneous Density
FM2L	Mixed	Late Seral: Small	8 - 14 in. DBH	Low Density/ Patchy
FM2M	Mixed	Late Seral: Small	8 - 14 in. DBH	Medium Density
FM3H	Mixed	Late Seral: Medium	14 - 20 in. DBH	High/ Homogeneous Density

Vegetation Code	Major Type	Size Description	DBH Range	Density Description
FM3L	Mixed	Late Seral: Medium	14 - 20 in. DBH	Low Density/ Patchy
FM3M	Mixed	Late Seral: Medium	14 - 20 in. DBH	Medium Density
FM4H	Mixed	Late Seral: Large	20 - 30 in. DBH	High/ Homogeneous Density
FM4L	Mixed	Late Seral: Large	20 - 30 in. DBH	Low Density/ Patchy
FM4M	Mixed	Late Seral: Large	20 - 30 in. DBH	Medium Density
FM5H	Mixed	OFS Candidate	>30 in. DBH	High/ Homogeneous Density
FM5L	Mixed	OFS Candidate	>30 in. DBH	Low Density/ Patchy
FM5M	Mixed	OFS Candidate	>30 in. DBH	Medium Density
NF	Non-Forest/ Other			

34 Appendix V – Longitudinal T_{max} Profiles for all Principal Streams

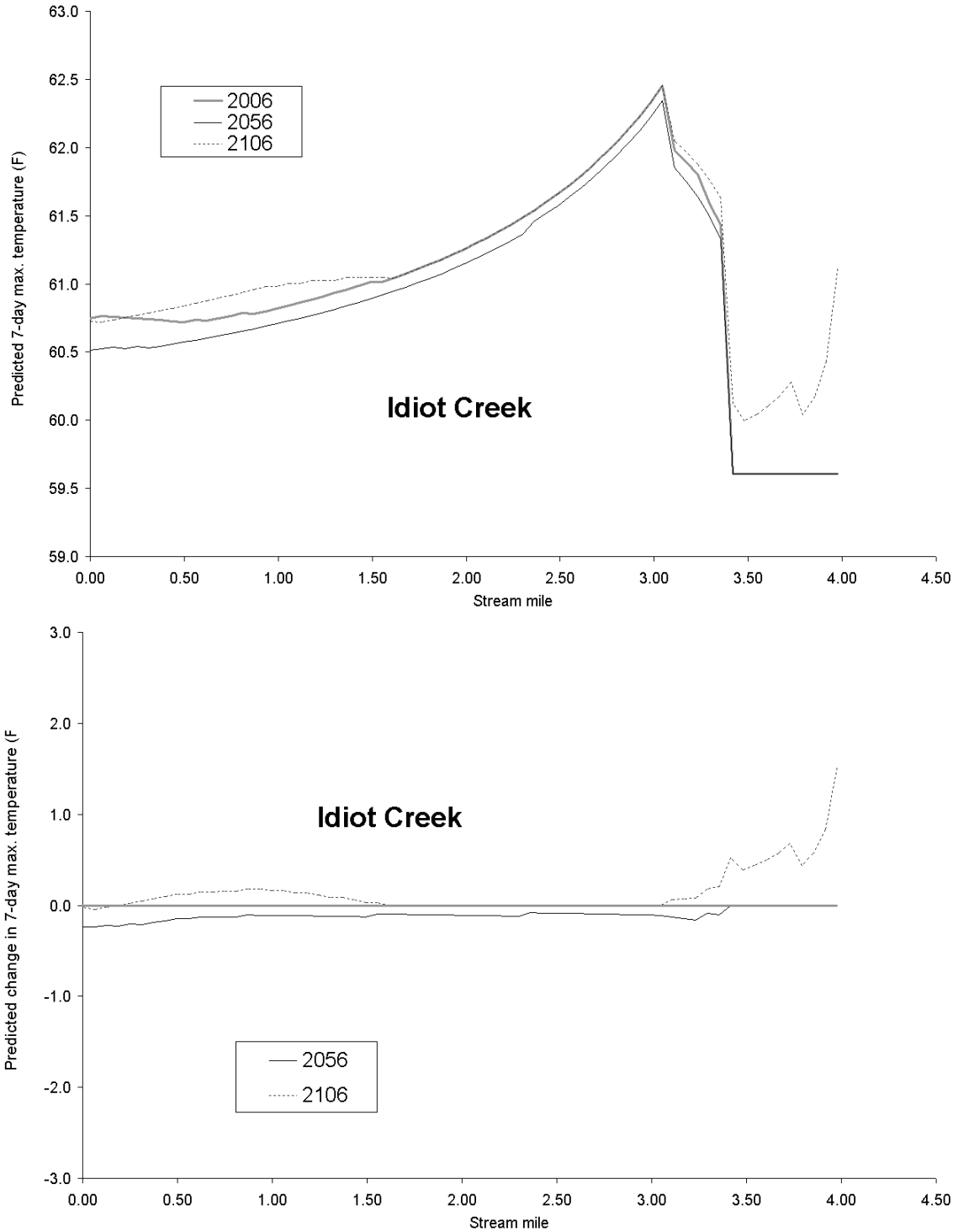

Figure 76. Longitudinal T_{max} profile, Idiot Creek. Top graphs shows predicted T_{max} values for current (2006) and future (2056 and 2106) scenarios. Bottom graphs shows difference between future and current scenarios.

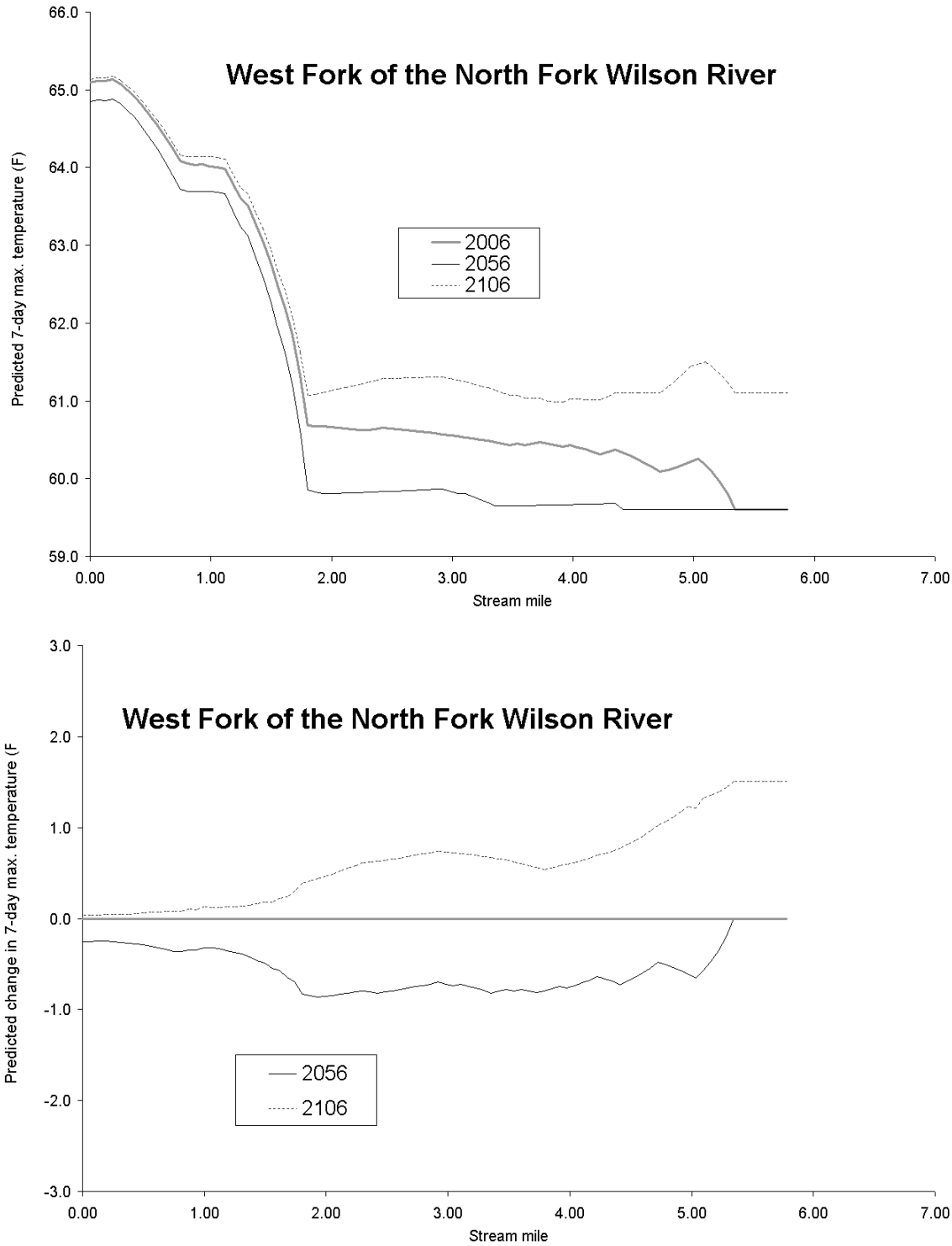

Figure 77. Longitudinal T_{max} profile, West Fork of the North Fork Wilson River. Top graphs shows predicted T_{max} values for current (2006) and future (2056 and 2106) scenarios. Bottom graphs shows difference between future and current scenarios.

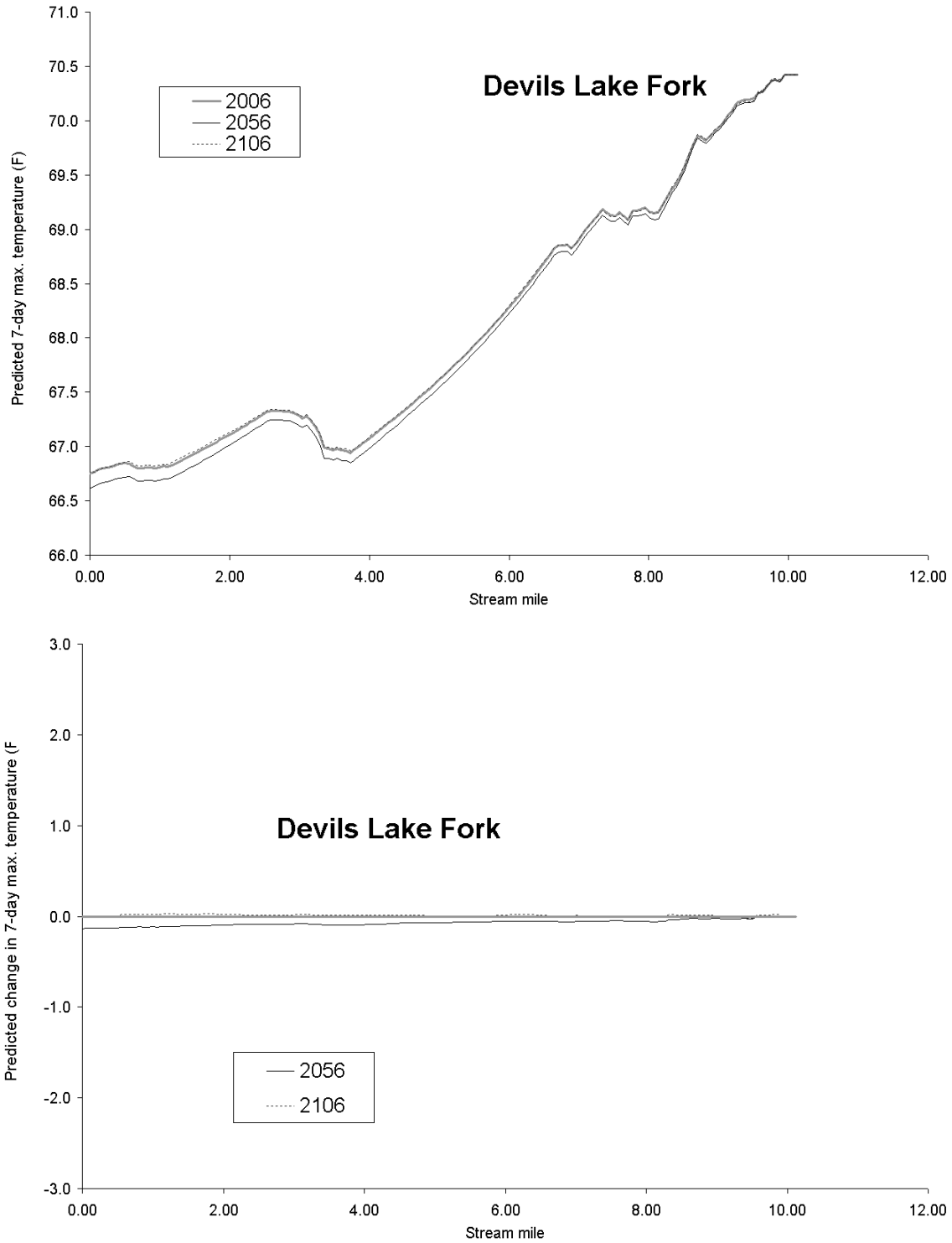

Figure 78. Longitudinal T_{max} profile, Devils Lake Fork Wilson River. Top graphs shows predicted T_{max} values for current (2006) and future (2056 and 2106) scenarios. Bottom graphs shows difference between future and current scenarios.

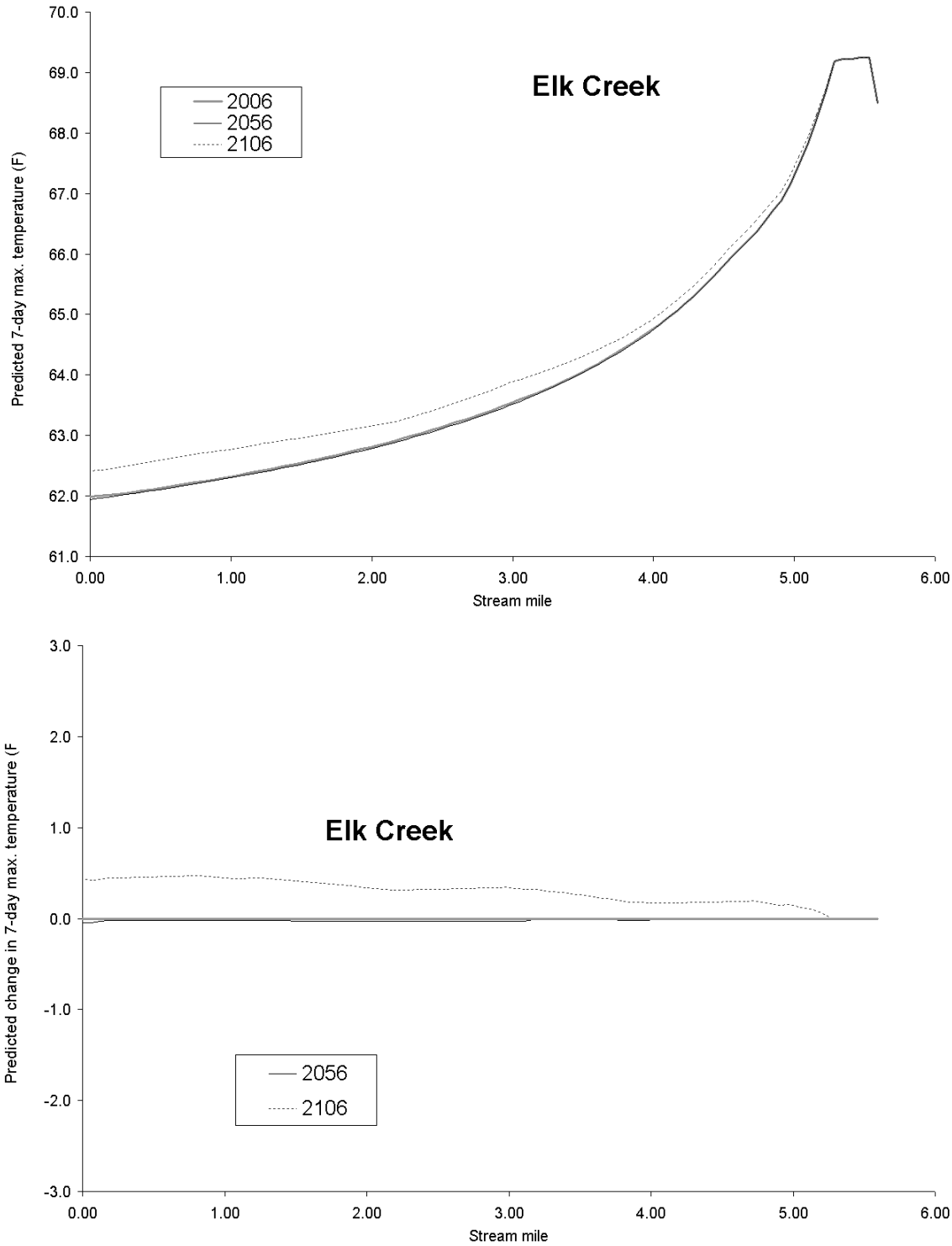

Figure 79. Longitudinal T_{max} profile, Elk Creek. Top graphs shows predicted T_{max} values for current (2006) and future (2056 and 2106) scenarios. Bottom graphs shows difference between future and current scenarios.

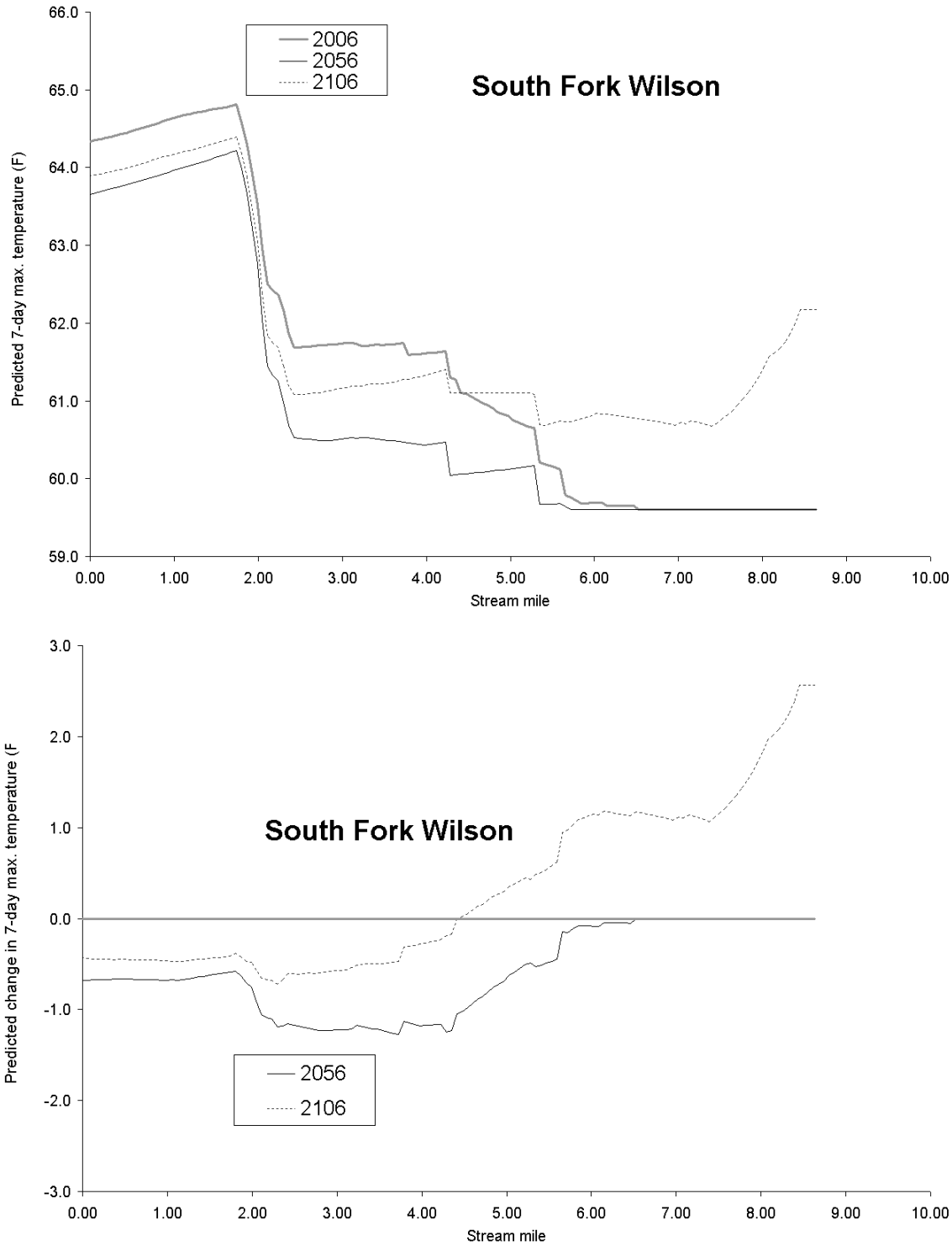

Figure 80. Longitudinal T_{max} profile, South Fork Wilson River. Top graphs shows predicted T_{max} values for current (2006) and future (2056 and 2106) scenarios. Bottom graphs shows difference between future and current scenarios.

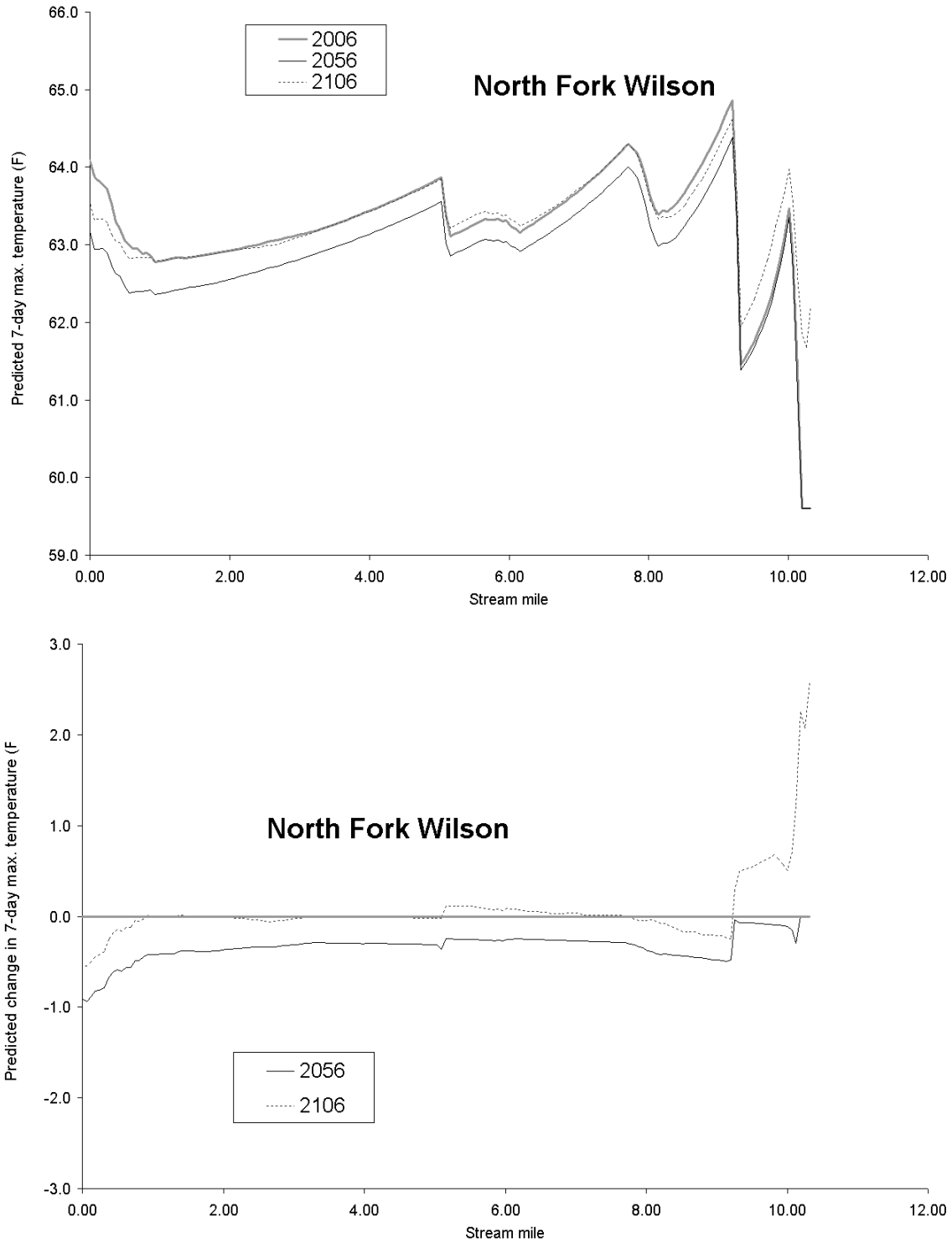

Figure 81. Longitudinal T_{max} profile, North Fork Wilson River. Top graphs shows predicted T_{max} values for current (2006) and future (2056 and 2106) scenarios. Bottom graphs shows difference between future and current scenarios.

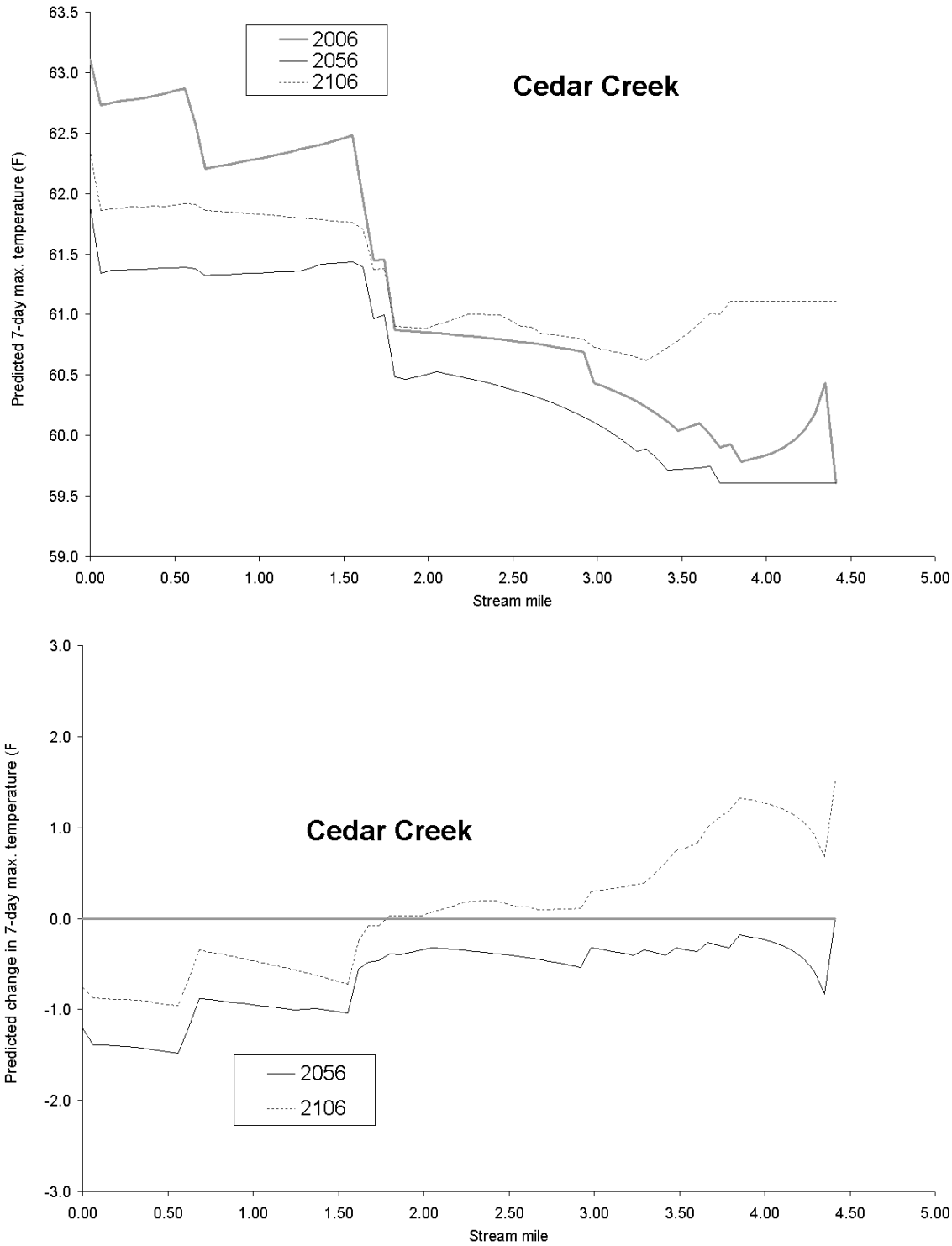

Figure 82. Longitudinal T_{max} profile, Cedar Creek. Top graphs shows predicted T_{max} values for current (2006) and future (2056 and 2106) scenarios. Bottom graphs shows difference between future and current scenarios.

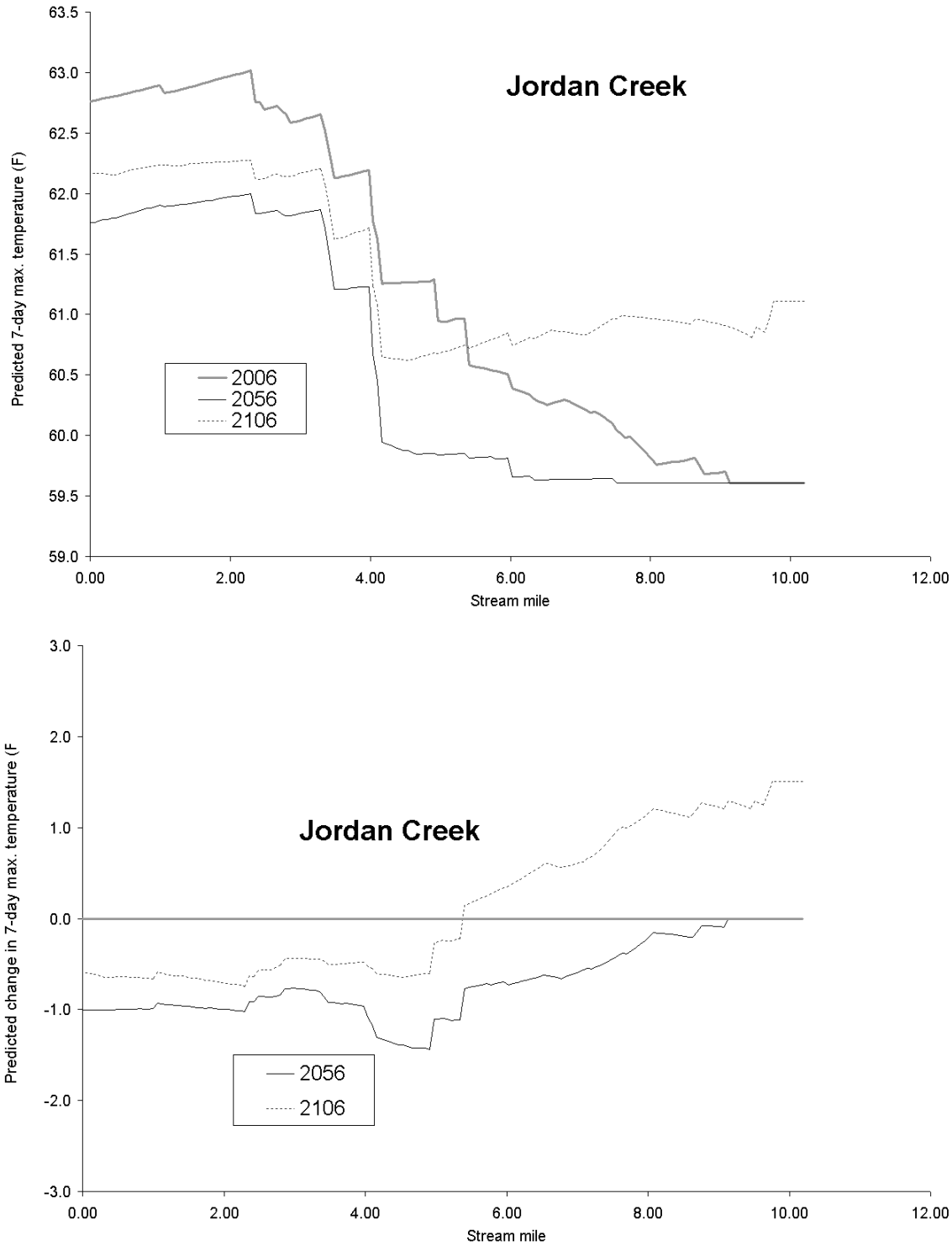

Figure 83. Longitudinal T_{max} profile, Jordan Creek. Top graphs shows predicted T_{max} values for current (2006) and future (2056 and 2106) scenarios. Bottom graphs shows difference between future and current scenarios.

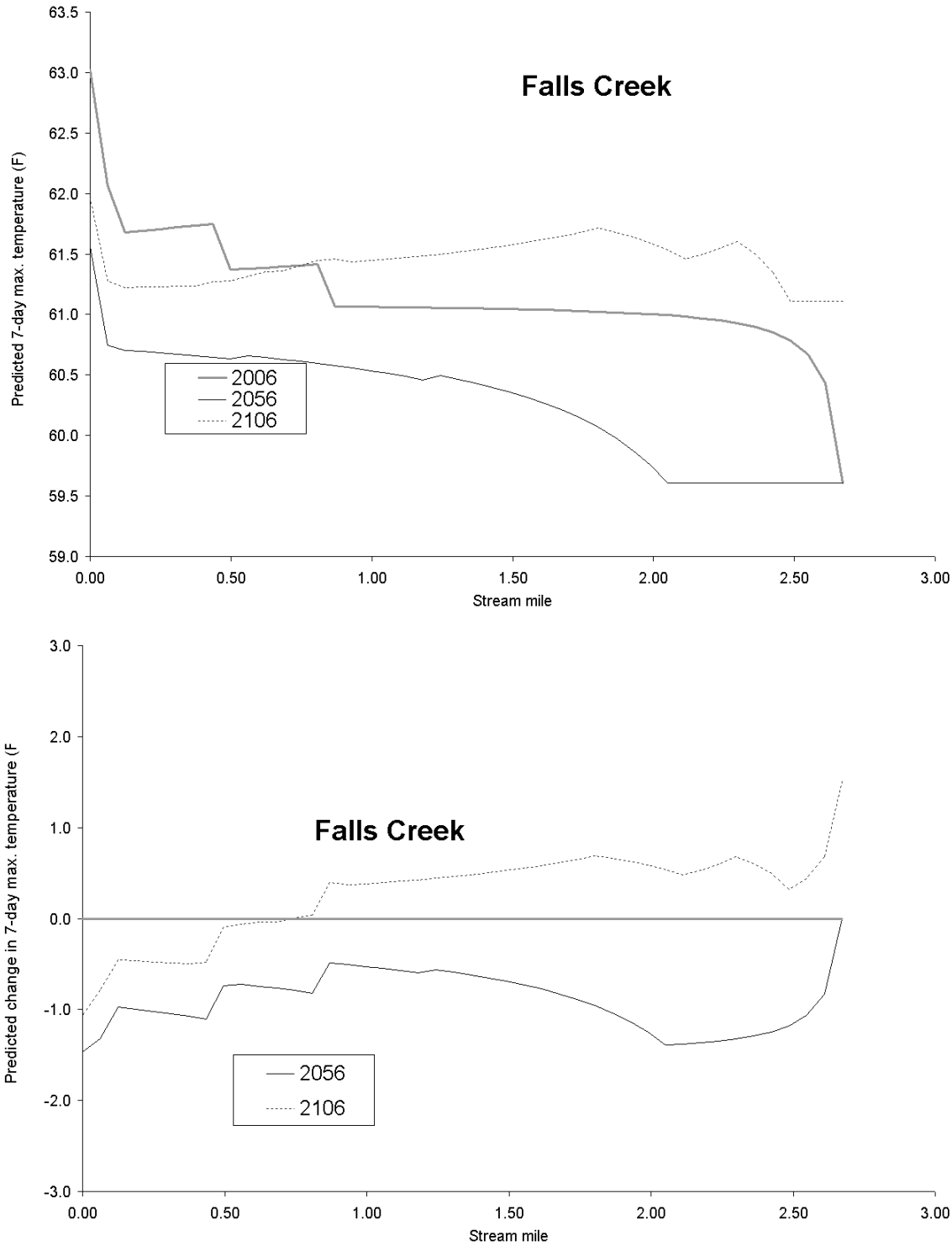

Figure 84. Longitudinal T_{max} profile, Falls Creek. Top graphs shows predicted T_{max} values for current (2006) and future (2056 and 2106) scenarios. Bottom graphs shows difference between future and current scenarios.

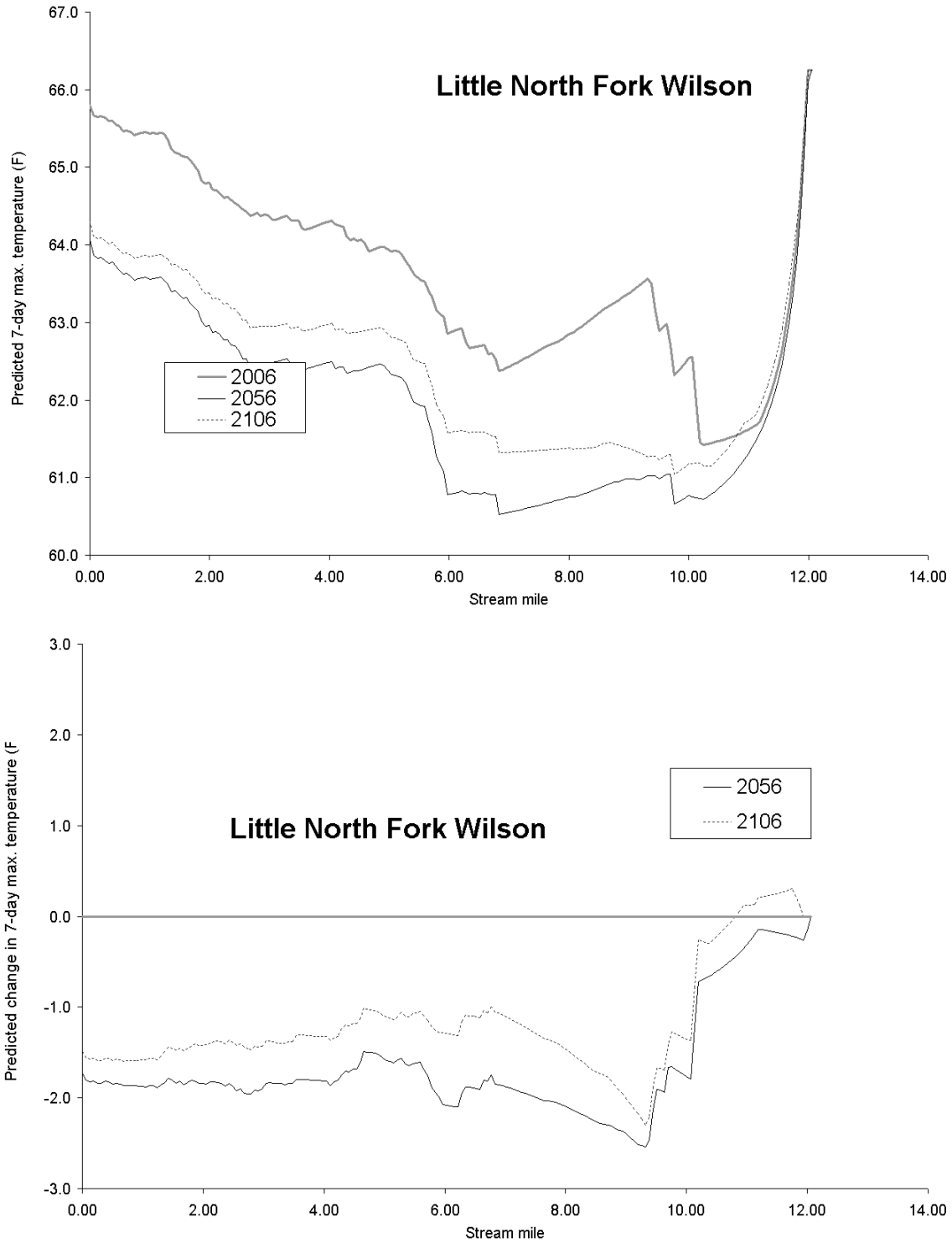

Figure 85. Longitudinal T_{max} profile, Little North Fork Wilson River. Top graphs shows predicted T_{max} values for current (2006) and future (2056 and 2106) scenarios. Bottom graphs shows difference between future and current scenarios.

35 Appendix W – List of Priority Dispersed Recreation Sites for Upgrade or Closure

Table 88. High priority dispersed camping sites recommended for upgrade or closure based on ODF-recorded human impact ratings of "High/Very High" (n=62). Site Code corresponds to the codes listed in ODF's dispersed campsite inventory database.

SITE CODE	Human Impact Comments	Overall Impact
TL008	Largest impact: pit riding.	Very High
TL016	Largest impacts: garbage, access road next to stream with no buffer.	Very High
TL019	Largest impact: stream running through site, carrying sediment and garbage directly into W. Fork Wilson River.	Very High
TL032	Largest impacts: heavy use, garbage dumping, and unmanaged OHV trail.	Very High
TL033	Largest impact: dumping of large items.	Very High
TL040	Largest impact: campsite on cliff over stream with no buffer.	Very High
TL050	Largest impacts: heavy use, vehicular erosion and rutting, and unnecessary road network.	Very High
TL051	Largest impacts: draft road to Wilson River, fire ring under high water mark, heavy use, vehicular erosion and rutting, and unnecessary road network.	Very High
TL052	Largest impacts: hazard trees, heavy use, vehicular erosion and rutting, and unnecessary road network.	Very High
TL061	Largest impacts: road to site crosses small stream and also provides unsecured access to the back of the foresty center. In addition, severe tree damage.	Very High
TL067	Largest impact: heavily rutted road with direct sediment drainage into river. Also, heavy use as a party spot with lots of garbage.	Very High
TL068	Largest impact: heavily rutted road with direct sediment drainage into river. Also, heavy use as a party spot with lots of garbage.	Very High
TL069	Largest impact: water traveling down road, pooling in camp site, and draining with sediment directly into river. Heavy use site.	Very High
TL070	Largest impacts: no buffer to stream, garbage. Safety issue: fire ring only a few feet from cliff being undercut by stream.	Very High
TL071	Largest impact: small stream running through campsite carrying sediment.	Very High
TL072	Largest impact: no buffer to stream.	Very High
TL076	Largest impact: 2 fire rings directly next to stream.	Very High
TL077	Largest impacts: lots of garbage, no buffer to stream, heavy use.	Very High
TL081	Largest impact: no buffer on steep bank to stream and waterfall.	Very High
TL092	Largest impacts: garbage, human waste, tree damage, OHV riding, little buffer to creek.	Very High

SITE CODE	Human Impact Comments	Overall Impact
TL104	Highest impact: erosion and severe rutted condition of access roads.	Very High
TL105	VERY HIGH IMPACT: 4wd tracks crossing creeks in at least 3 places. Road drainage not functioning. Deeply rutted meadow and unmanaged OHV access to forest. High volume of garbage.	Very High
TL117	Highest impact: fire rings under high water mark; camping right next to active salmon spawning stream. Also, plenty of garbage.	Very High
TL119	Largest impacts: heavy use, no buffer to stream, damaged trees, garbage.	Very High
TL128	Largest impacts: major access road rutting from vehicle traffic.	Very High
TL147	VERY HIGH IMPACT: severe rutting from vehicle traffic. Extensive section of road and campsite were flooded. Draft road provides OHV access to river bed.	Very High
TL148	Largest impact: access road and campsite on cliff edge above stream with no buffer. Also, can park on stream's edge because of draft road.	Very High
TL150	Largest impact: campsite on cliff's edge over stream at end of draft road. Safety concern.	Very High
TL126	Largest impacts: close proximity to stream and garbage.	High
FG029		High
FG039	largest impact = user created trails and mud pits	High
FG053		High
FG070		High
FG073	Largest impact = motorized user-created trail network	High
FG074	Lots of user created motorized trails surrounding the site.	High
FG092	Lots of garbage. Heavy amounts of tree damage. A little streamside erosion occurring.	High
FG101	Ax marks in trees. Many user created hiking and OHV trails on North side of site	High
TL009	Largest impact: pit riding.	High
TL011	Highest impact: fire ring under high water mark.	High
TL012	Highest impact: easy vehicle access to stream on legacy draft road.	High
TL024	Largest impact: 2 OHV access paths.	High
TL030	Largest impact: < 25 ft. from stream, heavy use.	High
TL039	Largest impact: heavy use.	High
TL041	Largest impacts: damaged trees, garbage, draft road access to streamside.	High
TL046	Largest impacts: unnecessary road network.	High
TL049	Largest impacts: heavy use, vehicular erosion and rutting, and unnecessary road network.	High
TL054	Largest impacts: unnecessary road network, vehicular erosion and rutting.	High
TL055	Largest impacts: unnecessary road network, vehicular erosion and rutting.	High

SITE CODE	Human Impact Comments	Overall Impact
TL056	Largest impacts: unnecessary road network, vehicular erosion and rutting.	High
TL057	Largest impacts: unnecessary road network, vehicular erosion and rutting.	High
TL058	Largest impacts: unnecessary road network, vehicular erosion and rutting.	High
TL059	Largest impacts: unnecessary road network, vehicular erosion and rutting.	High
TL060	Largest impacts: garbage, access to 2 unmanaged motorcycle trails up the creek drainages.	High
TL087	Largest impacts: garbage, vehicular rutting.	High
TL096	Highest impact: heavy use and close proximity to stream.	High
TL097	Largest impact: heavy use, close proximity to stream, and OHV trails.	High
TL101	Largest impact: garbage and highly rutted condition of access road.	High
TL103	Largest impacts: unbuffered access to stream and garbage.	High
TL107	Largest impact: access to multiple unmanaged OHV trails.	High
TL112	Fire hazard: nearby slash piles. Largest impact: pit riding.	High
TL139	Other impacts: large amount of spray-paint grafitti on trees and boulders, as well as carved grafitti on trees.	High
TL156	Largest impacts: no buffer to stream, damaged trees.	High

Table 89. High priority dispersed camping sites recommended for upgrade or closure based on proximity to a stream (<25ft; n=33). Site Code corresponds to the codes listed in ODF's dispersed campsite inventory database.

Site Codes for sites within 25 feet of a stream			
TL141	TL076	TL030	TL148
TL117	TL077	TL119	TL150
TL118	TL011	TL092	TL156
TL105	TL096	TL003	TL040
TL137	TL097	TL146	TL019
TL130	TL126	TL047	TL072
TL101	TL081	TL051	
TL070	TL016	TL147	

This page left intentionally blank.